Acta Oceanol. Sin., 2023, Vol. 42, No. 3, P. 1–18
https://doi.org/10.1007/s13131-022-2082-5
http://www.aosocean.com
E-mail: ocean2@hyxb.org.cn

Aliphatic biomarker signatures of early Oligocene–early Miocene source rocks in the central Qiongdongnan Basin: Source analyses of organic matter

Min Xu[1, 2, 3], Dujie Hou[1, 2, 3]*, Xiong Cheng[1, 2, 3], Jun Gan[4], Xinde Xu[4], Gang Liang[4], Wenjing Ding[5]

[1] School of Energy Resources, China University of Geosciences, Beijing 100083, China

[2] Key Laboratory of Marine Reservoir Evolution and Hydrocarbon Accumulation Mechanism, Ministry of Education, Beijing 100083, China

[3] Beijing Key Laboratory of Unconventional Natural Gas Geological Evaluation and Development Engineering, Beijing 100083, China

[4] Exploration and Development Resource Institute, Hainan Branch of China National Offshore Oil Corporation, Hainan 570300, China

[5] China National Offshore Oil Corporation (CNOOC) Research Institute Co., Ltd., Beijing 100028, China

Received 23 February 2022; accepted 28 June 2022

Abstract

The geochemical signatures of fifty-four rock samples and three supplementary drill stem test (DST) oils from the Yacheng-Sanya formations in the central Qiongdongnan Basin (CQB) were analysed. Reconstruction of the early Oligocene–early Miocene (36–16 Ma) palaeovegetation and source analyses of organic matter (OM) were conducted using aliphatic biomarkers in ancient sediments and DST oils. Both the interpreted aquatic and terrigenous OM contributed to the CQB source rocks (SRs) but had varying relative proportions. The four distribution patterns derived from *n*-alkanes, terpanes, and steranes are representative of four OM composition models of the Yacheng-Sanya SRs, including model A, model B, model C, and model D, which were classified based on the increasing contribution from terrigenous OM relative to aquatic OM. Some terrigenous higher plant-derived biomarkers, including oleanane, *des*-A-oleanane, C_{29} $\alpha\alpha\alpha$ 20R sterane, bicadinanes, the $C_{19}/(C_{19} + C_{23})$ tricyclic terpane ratio, and other *n*-alkane-derived ratios suggest that angiosperms had increased proportions in the palaeoflora from early Oligocene to early Miocene, and the bloom of terrigenous higher plants was observed during deposition of upper Lingshui Formation to lower Sanya Formation. These findings are consistent with the incremental total organic carbon and free hydrocarbons + potential hydrocarbons ($S_1 + S_2$) in the lower Lingshui-lower Sanya strata with a significant enrichment of OM in the E_3l_1-N_1s_2 shales. The maturity- and environment-sensitive aliphatic parameters of the CQB SRs and DST oils suggest that all the samples have predominantly reached their early oil-generation windows but have not exceeded the peak oil windows, except for some immature Sanya Formation shales. In addition, most of the OM in the analysed samples was characterised by mixed OM contributions under anoxic to sub-anoxic conditions. Furthermore, terrestrial-dominant SRs were interpreted to have developed mainly in the Lingshui-Sanya formations and were deposited in sub-oxic to oxic environments, compared to the anoxic to sub-anoxic conditions of the Yacheng Formation.

Key words: aliphatic biomarkers, early Oligocene–early Miocene, organic matter sources, palaeovegetation reconstruction, Qiongdongnan Basin

Citation: Xu Min, Hou Dujie, Cheng Xiong, Gan Jun, Xu Xinde, Liang Gang, Ding Wenjing. 2023. Aliphatic biomarker signatures of early Oligocene–early Miocene source rocks in the central Qiongdongnan Basin: Source analyses of organic matter. Acta Oceanologica Sinica, 42(3): 1–18, doi: 10.1007/s13131-022-2082-5

1 Introduction

The Qiongdongnan Basin, which is adjacent to south-eastern Hainan Island and located on the north-western continental shelf of the South China Sea, is one of the most prolific Cenozoic petroliferous basins along the continental margin of the South China Sea. The South China Sea is a relatively vast and profound marginal sea, the tectonic location of which is in the joint area shared by the Pacific and Tethys tectonic domains, and the South China Sea plays a role in connecting the Southeast Asia continent with the southwestern Pacific Ocean (Ding et al., 2021; Ren et al., 2011; Zhu et al., 2021). Due to its special geographical position, the South China Sea is very sensitive to variations in the global climate and palaeomarine environment (Webster, 1994), and these processes are closely related to the terrestrial organic matter (OM) influx (Ding et al., 2021; Liu et al., 2016b; Tamburini et al., 2003). Large amounts of fluvial sediments are transported along waterways and deposited primarily on the continental margins and slopes of marginal seas, usually forming either terminal sedimentary sinks or passageways to open-ocean regions (Liu et al., 2016b).

The Qiongdongnan Basin is a Cenozoic extensional basin based on pre-Paleogene igneous rocks, sedimentary rocks, and

Foundation item: The National Natural Science Foundation of China under contract No. 41872131.
*Corresponding author, E-mail: houdj313@163.com

metamorphic rocks (Huang et al., 2003; Lai et al., 2021; Li et al., 2020; Zhu et al., 2021). This basin is NE–SW-trending overall and covers a total area of approximately 65 000 km^2, nearly 70% of which is deep-water (water depths>300 m), and its exact longitudinal and latitudinal coordinates lie between 108°52′–110°47′E and 16°47′–19°00′N, respectively (Huang et al., 2016; Wang et al., 2015a) (Fig. 1). The Qiongdongnan Basin can be structurally divided into four first-order tectonic belts, including the northern depression, the central uplift, the central depression, and the southern uplift. Furthermore, it can be subdivided into 20 secondary tectonic units (e.g., the Songtao Uplift, Songnan Sag, Baodao Sag, Songnan Low Uplift, and Lingshui Sag, as shown in Fig. 1b).

The basin has experienced two tectonic evolution stages during the Cenozoic (Huang et al., 2016; Lai et al., 2021; Su et al., 2018), including the Paleogene rifting stage and the post-Paleogene depression stage. The Cenozoic depositional sequences in the Qiongdongnan Basin are recorded by five diverse successions, that is, Eocene lacustrine sediments, early Oligocene continental-to-marine transitional to semi-enclosed neritic successions, late Oligocene–mid-Miocene littoral-to-neritic facies, late Miocene–Pliocene littoral-to-bathyal deposits, and a Quaternary littoral sequence (Ding et al., 2021; Lai et al., 2021; Su et al., 2018; Zhu et al., 2021) (Fig. 1c, modified from Lai et al. (2021); Su et al. (2018)). The stratigraphy has been recorded through drilling, and the successive layers are as follows, from old to new: the late Eocene Lingtou Formation (E_2l), early Oligocene Yacheng Formation (E_3y), late Oligocene Lingshui Formation (E_3l), early Miocene Sanya Formation (N_1s), mid-Miocene Meishan Formation (N_1m), late Miocene Huangliu Formation (N_1h), Pliocene Yinggehai Formation (N_2y) and Quaternary Ledong Formation (Ql). The Yacheng and Lingshui formations can be trisected into $E_3y_{1\text{-}3}$ and $E_3l_{1\text{-}3}$, respectively, and the Sanya Formation can be dichotomized into N_1s_1 and N_1s_2. The regional tectonic features and sedimentary facies indicate that the palaeowater gradually deepened spatially from the northwest to the southeast and temporally from the early Oligocene to the Miocene in the Qiongdongnan Basin; in addition, the palaeovegetation compositions and source inputs of the ancient sediments changed similarly.

The Qiongdongnan Basin has experienced more than 40 years of petroleum exploration since the Y-9 well was first drilled in 1979. During recent decades, a sequence of giant gas fields and hydrocarbon-bearing structures has been established in this basin, including but not limited to the YA13-1, LS17-2, LS25-1, LS25-1 W, LS18-1, and LS18-2 gas fields, in which the YA13-1 gas field is the largest and first-discovered commercial gas field in the Qiongdongnan Basin (Xiao et al., 2006; Zhou et al., 2003). The other gas fields listed above are all located in the central depression, and the LS17-2 gas field is the largest among these fields; this field is located in a deep-water area and has an initial gas-in-place reserve of approximately 110×10^9 m^3 (Zhang et al., 2016; Zhu et al., 2021). Due to the tremendous sedimentary volumes

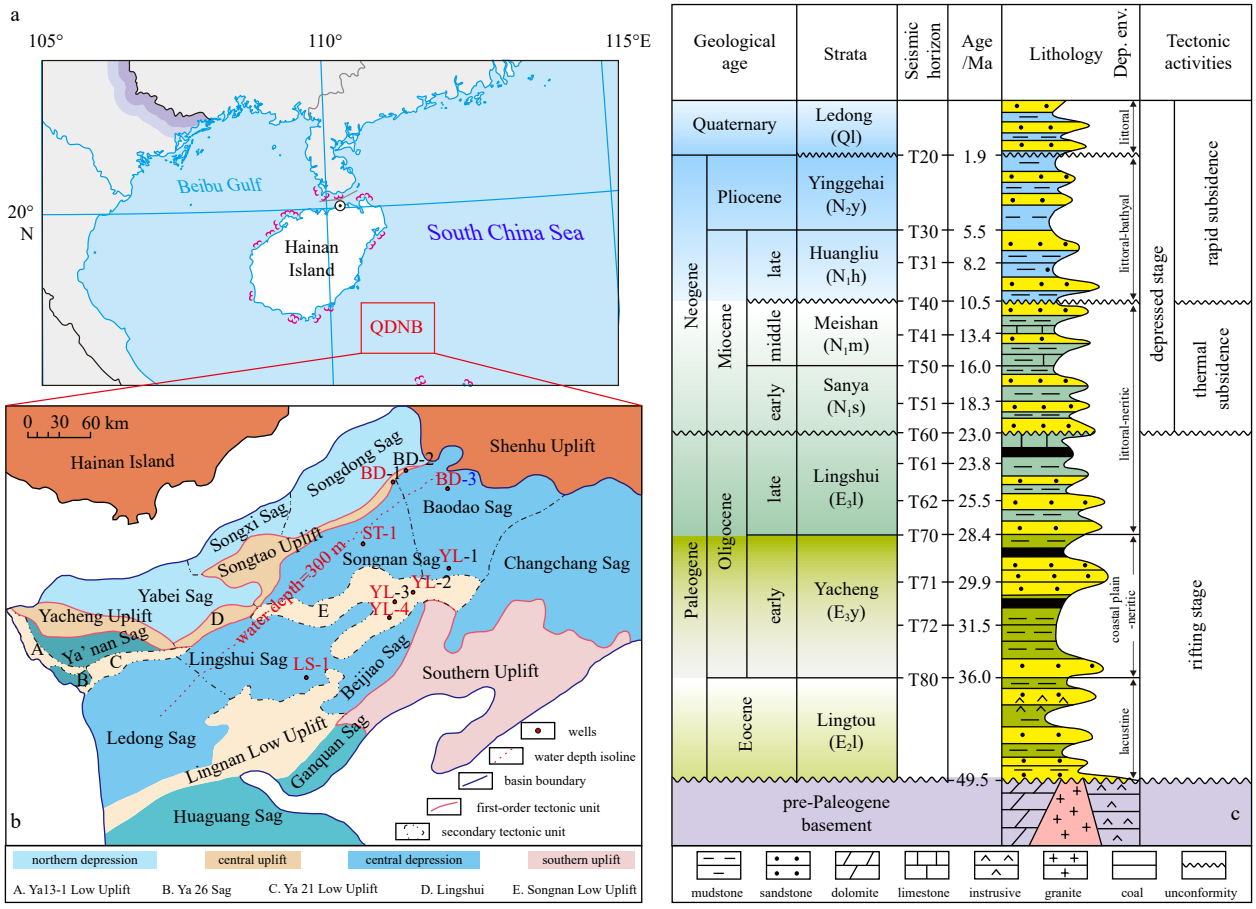

Fig. 1. Map showing the regional geological outline of the Qiongdongnan Basin (QDNB). a. Geographic location of the QDNB in the South China Sea. b. Schematic structure of the QDNB and location of associated wells, well names in black include cutting samples, names in red contain core/sidecore samples, and letters in blue indicate drill stem test oils involved. c. The stratigraphic column of QDNB. Dep. env. : depositional environment.

and extensive gas potentials in the Qiongdongnan Basin, this region has become an important exploration hotspot along the continental marginal basins of China (Zhu et al., 2021). In the last decade, numerous studies have been conducted on the Qiongdongnan Basin, predominantly concerning the petroleum geological conditions (Liu et al., 2016a; Wang et al., 2014a; Zhu et al., 2021), regional tectonic evolution (Ren et al., 2011; Wang et al., 2014b; Yang et al., 2022), petroleum and source rock geochemistry (Lai et al., 2021; Zhu et al., 2018, 2021), source rock developmental controls (Li and Zhang, 2017; Li et al., 2013; Miao et al., 2018), and sedimentary characteristics (Cao et al., 2017; Lei et al., 2019; Liu et al., 2016b; Ren et al., 2014; Wang et al., 2015a; Wu et al., 2018b); topics of specific focus include hydrocarbon-generation potentials of coal-bearing source rocks (SRs) (Huang et al., 2012, 2016; Lai et al., 2021; Li et al., 2012, 2020; Ren et al., 2015; Wang et al., 2020, 2021; Zhang et al., 2019) and natural gas-related research (Ding et al., 2018; Huang et al., 2012, 2016, 2017; Su et al., 2012, 2017, 2018; Wang et al., 2015c; Zhang et al., 2016).

The lower Oligocene-lower Miocene SRs in the central Qiongdongnan Basin (CQB) revealed by drilling are predominantly terrigenous-marine SRs, and this type of source rock is specific to continental marginal sedimentary basins. There has been an increase in research interest for terrigenous-marine SRs due to their great resource potential coupled with their wide distribution and large thickness in the South China Sea (Fan et al., 2021; Gao et al., 2018; Huang et al., 2016; Li and Zhang, 2017; Wang et al., 2015b). However, owing to the low-exploration stage of the deep-water region, where no more than 11 wells have been drilled into the lower Oligocene E_3y stratum thus far, the diverse OM composition models in the lower Oligocene–lower Miocene terrigenous-marine SRs have not been investigated in detail, and relatively few published studies have focused on the systematic reconstruction of palaeovegetation or palaeoenvironmental conditions during early Oligocene to early Miocene in the CQB or even in the South China Sea using geochemical parameters, especially few analyses have been conducted in combination with the latest petroleum exploration.

In previously published reports, Ding et al. (2021) discussed the palaeovegetation variations that occurred in response to the late Oligocene–early Miocene East Asian summer monsoon in the Ying-Qiong Basin and reconstructed the palaeovegetation and palaeoclimate during the late Oligocene–early Miocene in their study area. Wu et al. (2018a) analysed the palaeoenvironmental conditions of Oligocene SRs in the Baodao-Changchang sags based on evidence from organic geochemistry and palynology. Both Ding et al. (2021) and Wu et al. (2018a) generally agreed that tropical/subtropical angiosperm- and pteridophyte-derived OM dominated the Oligocene SRs and younger sediments (i.e., N_1s_1). However, there are some different opinions herein in the OM sources of the lower Oligocene-lower Miocene (Yacheng Formation-Sanya Formation) SRs. Given that, terrigenous-marine SRs are widespread in the CQB, and hence, terrestrial materials have been nonnegligibly incorporated into deposits in the CQB since the early Oligocene. Nevertheless, the composition models and traits of the OM involved in the original sediments, as well as ultimately preserved geochemical compounds, exhibited variations due to many controlling factors, e.g., the source materials, redox potential, and palaeowater depth, thereby finally representing the diversities of palaeovegetation and palaeoenvironmental conditions.

Numerous molecular biomarkers in petroleum and extractable hydrocarbons from ancient sediments can be linked with corresponding geologically ancient counterparts and have hence been widely used to reconstruct palaeovegetation compositions and depositional palaeoenvironments (Didyk et al., 1978; Ding et al., 2021; Hautevelle et al., 2006; Jiang et al., 2020; Jiang and George, 2018; La Croix et al., 2020). For example, the *n*-alkane ratios, including the wax index, terrigenous/aquatic ratio (TAR) and average chain length (ACL) (for all abbreviations and definitions of biomarkers, please see Table 1), are widely used to evaluate relative variations in terrigenous higher plant- versus aquatic-derived OM in original sediments (Blocho et al., 2021; Bourbonniere and Meyers, 1996; Ding et al., 2021; Hoş-Çebi, 2017; Jiang and George, 2018, 2019; Peters et al., 2005; Samad et al., 2020). Tricyclic terpanes ($<C_{30}$) seem to derive from a regular C_{30} isoprenoid, which could be constituents in prokaryotic membranes, and hopanes appear to originate from precursors in bacterial membranes; moreover, tricyclic terpanes are thought to be more resistant to thermal maturation and biodegradation than hopanes (Ourisson et al., 1979, 1982; Peters et al., 2005). Ding et al. (2021) have firstly defined the angiosperm-related indicator (oleanane + *des*-A-oleanane + taraxastane)/C_{30} $\alpha\beta$ hopane [(O + DAO + Ta)/C_{30} H]. Bicadinanes, including cis-cis-trans-bicadinane (W), trans-trans-trans-bicadinane (T), and R, are pentacyclic triterpanes derived from the dammar-type resins of tropical angiosperms, such as *Dipterocarpaceae* plants (Murray et al., 1997; Nytoft et al., 2010; Van Aarssen et al., 1992); these biomarkers were first detected by Grantham et al. (1983) in South Asian oils. Steranes are sterol-derived cycloalkanes derived from ancient eukaryotic photosynthetic algae and higher plants; the distribution patterns and relative abundances of regular steranes are source-related and generally indicative of the sedimentary environment (Ding et al., 2021; Jiang and George, 2018; Peters et al., 2005); pregnanes and homopregnanes were identified as the predominant steranes in ancient sediments deposited under hypersaline environments (Ten Haven et al., 1985), and the relative abundances of pregnanes compared with regular steranes tend to increase with incremental thermal maturity (Wingert and Pomerantz, 1986). The ratio of pristane (Pr) versus phytane (Ph), the two most common aliphatic isoprenoids, has been widely applied to indicate depositional environments (Didyk et al., 1978; Large and Gize, 1996; Ten Haven et al., 1988), although the Pr/Ph ratio is susceptible to thermal maturation (Albrecht et al., 1976; Peters et al., 2005; Vuković et al., 2016). The carbon preference index (CPI), the odd-to-even predominance (OEP) and the Ts/(Ts + Tm) ratio can be applied to evaluate the mature stage of SRs and oils but are also inescapably influenced by the variations in parent materials and the depositional environment (Ding et al., 2021, 2022; Jiang and George, 2018; Seifert and Moldowan, 1978; Xu et al., 2022). Furthermore, maturity-sensitive stereoisomers of hopanes and steranes are widely used to assess the thermal maturity of original sediments and petroleum; configurational isomerization occurs only when cleavage and renewed formation of the bonds has resulted in an inverted configuration in contrast with the original asymmetric centre; the R and S isomeric configurations of asymmetric carbon atoms in acyclic chains generally have similar thermal stabilities, while asymmetric centres that are part of a saturated ring system usually show two configurations (α and β) with entirely distinct thermal stabilities due to steric forces imposed by a rigid cyclic structure (Peters et al., 2005).

In this paper, aliphatic biomarkers obtained from extractable hydrocarbons and drill stem test (DST) oils were predominantly used, including oleanane, 10β(H)-*des*-A-oleanane, 10β(H)-*des*-A-lupane, 10β(H)-*des*-A-ursane, taraxastane, bicadianes, C_{19}–C_{24} tricyclic terpanes, C_{24} tetracyclic terpane, and C_{27}–C_{29} regular

Table 1. Abbreviations and definitions for some geochemical parameters mentioned in the text

Abbreviation	Definition
$CPI_{22\text{-}32}$	carbon preference index=2(C_{23}+C_{25}+C_{27}+C_{29}+C_{31})/(C_{22}+2C_{24}+2C_{26}+2C_{28}+2C_{30}+C_{32}) alkanes
OEP	odd-to-even predominance=$[(C_{max-2}+6\times C_{max}+C_{max+2})/(4C_{max-1}+4C_{max+1})]^{(-1)^{max-1}}$ alkanes
Wax index	(C_{21}+C_{22})/(C_{28}+C_{29}) alkanes
TAR	terrigenous/aquatic ratio=(C_{27}+C_{29}+C_{31})/(C_{15}+C_{17}+C_{19}) alkanes
$ACL_{15\text{-}33}$	average chain length=$\sum(n\times Cn)/\sum C_n$, n is among 15–33
Pr	pristane
Ph	phytane
C_{19}/(C_{19}+C_{23}) TT	C_{19}/(C_{19}+C_{23}) tricyclic terpanes
C_{23}/C_{21} TT	C_{23}/C_{21} tricyclic terpanes
C_{24} TeT/C_{23}TT	C_{24} tetracyclic terpane/C_{23} tricyclic terpane
Ts/(Ts+Tm)	C_{27} 18α(H)-22,29,30-trisnorneohopane/(C_{27} 17α(H)-22,29,30-trisnorhopane + C_{27} 18α(H)-22,29,30-trisnorneohopane)
C_{29} Ts/C_{29} H	18α-30-neohopane/C_{29} $\alpha\beta$ norhopane
C_{29} H/(H+M)	C_{29} $\alpha\beta/(\alpha\beta+\beta\alpha)$ norhopanes
C_{30} H/(H+M)	C_{30} $\alpha\beta/(\alpha\beta+\beta\alpha)$ hopanes
C_{31}/C_{30} H	C_{31} $\alpha\beta$ homohopane/ C_{30} $\alpha\beta$ hopanes
C_{31} 22S/(22S+22R) H	C_{31} $\alpha\beta$ 22S/(22S+22R) homohopanes
O/C_{30} H	oleanane/C_{30} $\alpha\beta$ hopane
GA/C_{30} H	gammacerane/C_{30} $\alpha\beta$ hopane
DAO/C_{30} H	*des*-A-oleanane/C_{30} $\alpha\beta$ hopane
Ta/C_{30} H	taraxerane/C_{30} $\alpha\beta$ hopane
(O+DAO+Ta)/C_{30} H	(oleanane+*des*-A-oleanane+taraxerane)/C_{30} $\alpha\beta$ hopane
(W+T)/C_{30} H	(cis-cis-cis-bicadinane+trans-trans-trans-bicadinane)/C_{30} $\alpha\beta$ hopane
T/$\sum C_{29}$ steranes	trans-trans-trans-bicadinane/C_{29} ($\alpha\alpha\alpha$ 20S+$\alpha\beta\beta$ 20R+$\alpha\beta\beta$ 20S+$\alpha\alpha\alpha$ 20R) steranes
C_{27}/C_{29} $\alpha\alpha\alpha$ 20R steranes	C_{27} $\alpha\alpha\alpha$ 20R sterane/C_{29} $\alpha\alpha\alpha$ 20R sterane
C_{29} 20S/(20R+20S) steranes	C_{29} $\alpha\alpha\alpha$ 20S/(20R+20S) steranes
C_{29} $\beta\beta/(\alpha\alpha+\beta\beta)$ steranes	C_{29} $\alpha\beta\beta/(\alpha\alpha\alpha+\alpha\beta\beta)$ 20R steranes

steranes. The latest test data from the new BD-3 drilling well were applied to extend the sample capacity. All above steps are prerequisites for systematically reconstructing the early Oligocene-early Miocene palaeovegetation and palaeoenvironmental conditions and ascertaining OM sources of terrigenous-marine SRs from the Yacheng-Sanya formations in the CQB.

2 Materials and methods

2.1 *Samples*

All the materials and samples used in this work were collected from the Hainan Branch of China National Offshore Oil Corporation (CNOOC) Co., Ltd. Sufficient samples were obtained for this study, including 30 cuttings and 24 sidecores derived from 9 wells in the CQB, among which 15 samples were from the N_1s stratum, 28 samples were from the E_3l stratum and 11 samples were from the E_3y stratum. In addition, 3 DST oils from Well BD-3 in the E_3l_3 stratum were included in this study. The details of representative rock samples obtained from 9 wells are shown in Table 2. The locations of the wells referred to in this paper are illustrated in Fig. 1b.

2.2 *Analytical methods*

Before their soluble hydrocarbons were extracted, we pretreated all rock samples by washing them with deionized water, wiping them with ethanol, powdering the samples to less than 100 mesh, and performing Soxhlet extraction for 72 h using chloroform. The following method to separate aliphatic hydrocarbons from the extractable organic matter (EOM) and crude oils was discussed in detail in Xu et al. (2022). Then, the aliphatic hydrocarbon fractions were analysed using the gas chromatography-mass spectrometry (GC-MS) method to determine the geochemical signatures, further reconstruct early Oligocene-early Miocene palaeovegetation and ascertain the sources of OM in the lower Oligocene–lower Miocene SRs. The GC-MS was performed on an Agilent 7890A GC apparatus equipped with a DB-5ms fused silica capillary column (with a 60 m×0.25 mm internal diameter and a film thickness of 0.25 μm) associated with an Agilent 5975C mass selective detector (with an ionization energy of 70 eV). The vapourization temperature in the inlet was set to 300°C, and the samples were injected in splitless mode using helium as the carrier gas at a stable flow velocity of 1.5 mL/min. The initial oven temperature was maintained at 50°C for 1 min, then programmed to 120°C at 20°C/min and further increased to 300°C at 2°C/min and maintained for 30 min. The samples were detected in full-scan mode. Additionally, the compound abundance normalization and calculation steps were performed on Chemstation based on the peak areas integrated into the mass chromatograms.

3 Results

3.1 *n-Alkanes and isoprenoids*

As illustrated in the *m/z* 85 mass chromatograms, the distributions of *n*-alkanes and isoprenoids in the aliphatic hydrocarbon fractions differed among SRs from the lower Oligocene E_3y to lower Miocene N_1s strata (Fig. 2). The *n*-alkanes of these rock samples exhibited a range of carbon numbers from C_{12} to C_{39},

Table 2. Detailed information and bulk geochemical parameters of representative rock samples from nine wells in the Qiongdongnan Basin

Sample ID	Well	Formation	Depth/m	Type	Lithology	TOC/%	(S_1+S_2)/(mg·g^{-1})	*Ro*/%	T_{max}/°C
R1	BD-1	N_1s_1	2 537	cutting	shale	0.44	0.65	0.61	434
R2	BD-1	N_1s_2	2 669	cutting	shale	0.72	1.03	0.63	437
R3	BD-1	E_3l_1	3 249	cutting	silty muds.	0.82	2.28	0.71	443
R4	BD-1	E_3l_2	4 183–4 221	cutting	shale	0.93	1.58	0.84	447
R5	BD-1	E_3l_3	4 599–4 601	cutting	silty muds.	0.58	1.02	0.84	451
R6	BD-2	E_3l_1	2 888.2–2 896.2	cutting	shale	0.50	0.52	0.71	435
R7	BD-2	E_3l_3	3 326.2–3 330.2	cutting	shale	0.52	0.5	0.76	437
R8	BD-2	E_3y_1	3 998.2–4 004.2	cutting	shale	0.98	0.67	1.03	451
R9	BD-3	E_3l_3	2 615.7	sidecore	shale	0.201	0.51	n.d.	440
R10	BD-3	E_3y_1	3 076.7	sidecore	shale	0.317	0.61	n.d.	445
R11	BD-3	E_3y_3	3 498.7	sidecore	shale	0.529	0.51	n.d.	446
R12	LS-1	E_3l	2 357.2	sidecore	shale	0.9	2.74	0.42	431
R13	ST-1	N_1s	2 719.2	sidecore	siltstone	n.d.	0.87	n.d.	n.d.
R14	YL-1	N_1s_2	1 255	sidecore	shale	n.d.	1.43	n.d.	423
R15	YL-1	E_3l_2	2 051–2 053	cutting	shale	n.d.	n.d.	n.d.	n.d.
R16	YL-1	E_3l_3	2 133.5	sidecore	siltstone	n.d.	0.69	n.d.	n.d.
R17	YL-2	N_1s	1 105.5	sidecore	shale	n.d.	2.54	n.d.	n.d.
R18	YL-2	E_3y	1 125.5	sidecore	siltstone	n.d.	1.28	n.d.	n.d.
R19	YL-3	N1s	992–996	cutting	shale	n.d.	n.d.	n.d.	n.d.
R20	YL-3	E_3y	1 024.5	sidecore	shale	n.d.	12.78	n.d.	406
R21	YL-4	E_3y_1	680.8	sidecore	siltstone	n.d.	0.91	n.d.	n.d.
O1	BD-3	E_3l_3	2 618.1–2 680.5	oil	DST	n.d.	n.d.	n.d.	n.d.
O2	BD-3	E_3l_3	2 618.1–2 680.5	oil	DST	n.d.	n.d.	n.d.	n.d.
O3	BD-3	E_3l_3	2 618.1–2 680.5	oil	DST	n.d.	n.d.	n.d.	n.d.

Note: R*x* and O*x* point to rock samples and drill stem test oils, respectively. "*x*" is the number of each representative sample; "Depth" points to buried depth of each sample with deduction of water-depth; TOC: total organic carbon; S_1+S_2: free hydrocarbons+potential hydrocarbons; *Ro*: vitrinite reflectance; T_{max}: temperature of maximum hydrocarbon generation rate; muds.: mudstone; n.d.: no data.

and four *n*-alkane distribution patterns were present: (1) a unimodal distribution pattern with an anteverted maximum $\leqslant C_{21}$, which was widespread in the E_3y-N_1s SRs represented in samples from the E_3l stratum of Well BD-1, with a 3 881.0–3 889.5-m sidecore, and BD-2, with 3 326.2–3 330.2-m cuttings (Fig. 2a); (b) a unimodal, approximately symmetric pattern with a maximum between C_{19} and C_{25}, which was predominantly present in E_3y–E_3l SRs, e.g., the sidecore samples of LS-1 at 2 357.2 m and of BD-3 at 3 076.7 m from the E_3l and E_3y strata, respectively (Fig. 2b); (3) a bimodal model with maxima at $C_{15\text{-}20}$ and $C_{24\text{-}27}$, which were principally found in E_3y-E_3l strata, for example, in shales from well BD-1 with 3 203–3 205-m cuttings from E_3l_1 and from Well YL-4 with a 680.8-m sidecore from E_3y_1, the presence of unresolved complex mixture humps in these two representative samples indicated that the samples have undergone moderate biodegradation (Ahmed et al., 2012), as was validated by the prior loss of light-molecular-weight less than C_{17} *n*-alkanes attributed to the inclination of the low carbon number of *n*-alkanes to lose their variable contents (Alkhafaji, 2021; Fazeelat et al., 2011; Galarraga et al., 2010) (Fig. 2c); and (d) a unimodal distribution model with moderate OEP at high molecular weights, which mainly occurred in the E_3l-N_1s SRs, for instance, in the cutting samples obtained from Well BD-1, N_1s_1 (2 537 m) and N_1s_2 (2 669 m) strata (Fig. 2d). The *n*-alkane distribution patterns illustrated different input proportions from terrestrial higher plant- and aquatic-derived OM, and the four patterns correspondingly represented four diverse OM composition models of the lower Oligocene-lower Miocene SRs in the study area, that is, model A, model B, model C, and model D.

Light-molecular-weight *n*-alkanes ($\leqslant C_{17}$) in aliphatic hydrocarbon fractions are inclined to stem from lower aquatic organisms, including algae, while long-chain odd *n*-alkanes ($\geqslant C_{27}$) are chiefly derived from the leaf wax components of terrigenous higher plants (Bourbonniere and Meyers, 1996; Peters et al., 2005). Generally, marine-sourced organic compounds have lower ACL values of 14 to 24, while terrestrial higher plant-derived organic components have higher ACL values ranging from 21 to 39 (Blocho et al., 2021; Eglinton and Hamilton, 1967; Jeng, 2006). Taking chain lengths 15 to 33 into account, the ACL values in the N_1s SRs ranged from 18.15 to 26.70, those in the E_3l SRs were in a range of 18.48–25.61 and those in the Yacheng SRs had a range of 20.44–24.29, showing a slight increase in the peak ACL values from E_3y to N_1s and the presence of moderate values, indicating mixed organic component inputs with some marine-over-terrestrial OM predominance. The $CPI_{22\text{-}32}$ values of all 54 rock extracts ranged from 0.84 to 1.30, with an average of 1.07, and the OEP had an approximate range of 0.70–1.38 (average of 1.03); in four samples present in the N_1s SRs, the values of these two parameters were higher than 1.20, indicating low maturity and higher plant inputs, while the other CPI values close to one are thought to have been caused by the dominant input of marine microorganisms and/or recycled OM (Kennicutt et al., 1987) or thermal maturation (Peters et al., 2005). The wax index values of all 54 samples were between 0.31 and 8.09, approximately 20.4% of which were lower than 1.0, and these samples were from the E_3l–N_1s strata, also suggesting the noticeable contribution of terrigenous higher plant-derived OM, while the wax index in the E_3y SRs ranged from 1.44 to 5.87, indicating lower contributions of terrigenous OM compared to the E_3l and N_1s strata discussed above. The *n*-alkanes of the aliphatic hydrocarbon fractionations

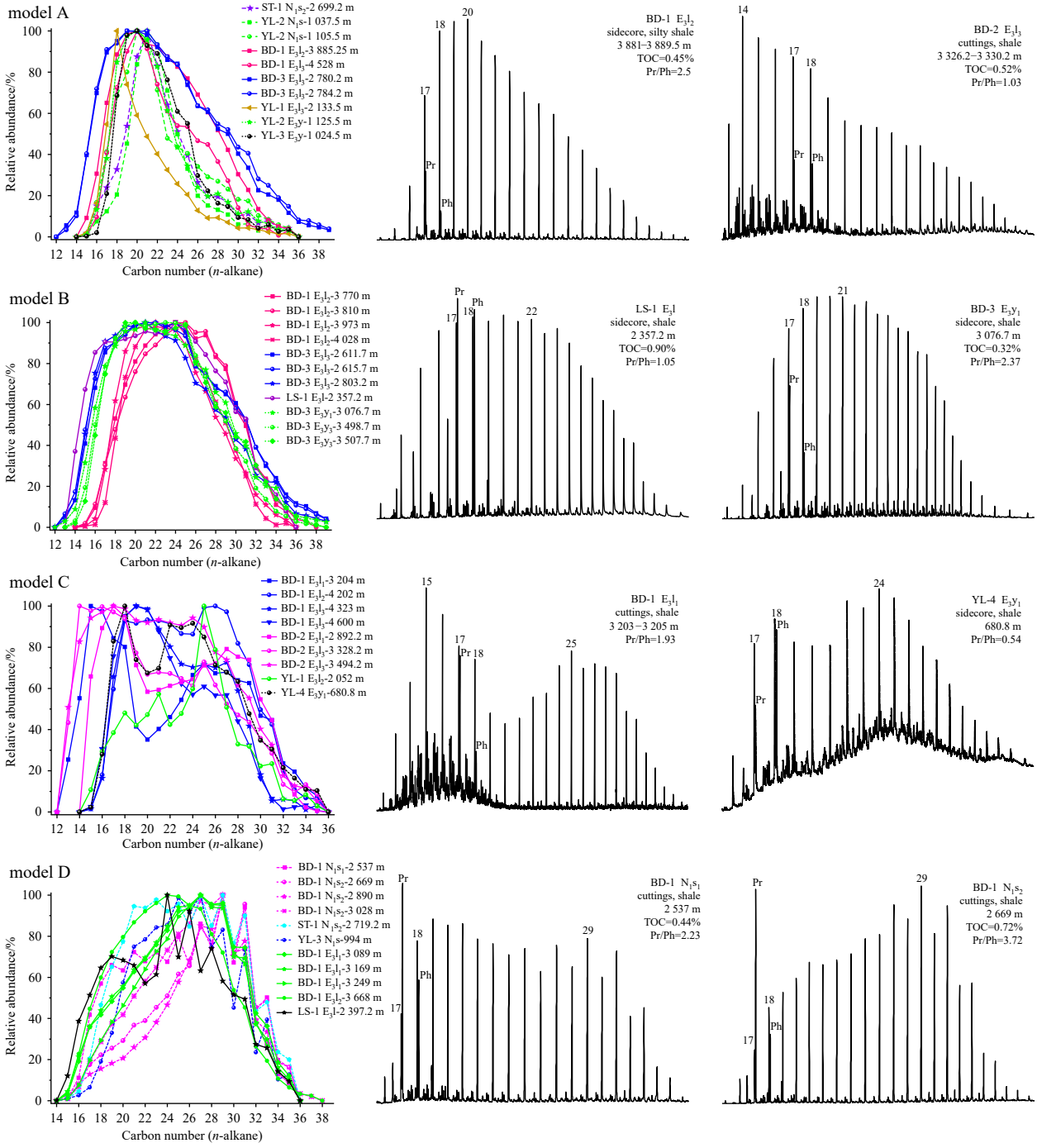

Fig. 2. Normalized *n*-alkane profiles of four distribution patterns for the early Oligocene to early Miocene source rocks from the Qiongdongnan Basin and partial *m/z* 85 mass chromatograms of the aliphatic hydrocarbon fractions showing the distributions of *n*-alkanes and isoprenoids in the representative samples for each pattern. Numbers in each figure represent carbon numbers of *n*-alkanes; Pr: Pristane; Ph: Phytane.

of the N_1s SRs exhibited large TAR values from 0.08 to 8.03, while the ranges of this index in the E_3l and E_3y strata were 0.10–4.46 and 0.20–3.29, respectively.

Among the 54 rock extracts examined in this paper, the Pr/Ph ratios were mostly less than 3.0, and only seven samples exhibited Pr/Ph values larger than 3 (within the range of 3.12–4.18, with an average of 3.63), six of which were obtained from Well BD-1 in the upper Lingshui Formation (E_3l_1) and the lower Sanya Formation (N_1s_2). High Pr/Ph values (>3) indicated obvious terrigenous OM inputs under oxic depositional environments (Peters et al., 2005). Specifically, a low Pr/Ph ratio (<0.8) points to an anoxic depositional environment that is generally related to hypersaline or carbonate conditions (Peters et al., 2005). In this study, approximately 26% of all analysed samples had Pr/Ph values<0.8, corresponding to the period throughout the Oligocene to early Miocene. Additionally, the measured isoprenoid/*n*-alkane ratios were indicative of both the thermal maturity and depositional environment of OM in SRs and oils (Peters et al., 1999, 2005). The cross-plot of Ph/nC_{18} versus Pr/nC_{17} shows that the E_3y-N_1s SRs were deposited in mixed and varied environments containing

partial Type-II OM in a reducing environment and Type-III OM in an oxidizing environment, as well as mixed OM types in transitional environments (Fig. 3). The aliphatic isoprenoids of the N_1s SRs exhibited large-scale Pr/Ph ratio variations (0.27–4.18) and Pr/nC_{17} ratio variations (0.28–5.46), among which the lowest Pr/Ph values observed in the YL-3 shales were caused by the strong biodegradation of light molecular *n*-alkanes (<C_{18}). In the upper Oligocene SRs, the Pr/Ph ratios ranged from 0.45 to 3.88, the Pr/nC_{17} ratios exhibited a similar range of 0.41–3.37, and the Ph/nC_{18} ratios ranged from 0.18 to 2.17. However, the isoprenoid-related ratios in the rock extracts derived from E_3y were lower than those in the overlying strata, with Pr/Ph ratios ranging from 0.23 to 2.37, Pr/nC_{17} ratios ranging from 0.22 to 0.79, and Ph/nC_{18} ratios ranging from 0.15 to 1.07.

Overall, the *n*-alkane ratios and isoprenoid characteristics described above illustrated the increasing trend of terrigenous OM input from the E_3y stratum to the N_1s stratum.

3.2 *Terpanes*

Tricyclic terpanes (TTs, for the compound structure see I in Appendix), C_{24} tetracyclic terpane (TeT; II), and hopanes (pentacyclic terpanes containing 27–35 carbon atoms; III), which are the common terpane types in the aliphatic hydrocarbon fractions of the E_3y-N_1s SRs within the CQB, together with oleanane-derived pentacyclic triterpanes, e.g., angiosperm-derived biomarkers including oleanane (IV), *des*-A-oleanane (V), *des*-A-lupane (VI), *des*-A-ursane (VII) and taraxastane (VIII), contribute to the terpane fingerprint (monitored in *m/z* 191, Fig. 4), which can indicate the depositional environment of ancient sediments and OM input (Peters et al., 2005); in contrast, diterpenoids are in minute abundance or are not detectable by GC-MS.

The terpane distribution profiles present in the *m/z* 191 mass chromatograms were different in the four OM composition models interpreted in Section 3.1; in particular, a lower relative content of TTs compared to hopanes was present in model A, in contrast with the other three models. The earlier eluted compounds in *m/z* 191 mass chromatograms included TTs, *des*-A-oleanane, *des*-A-lupane, *des*-A-ursane, and C_{24} TeT, and their distribution profiles reflected in model A were characterized by a unimodal

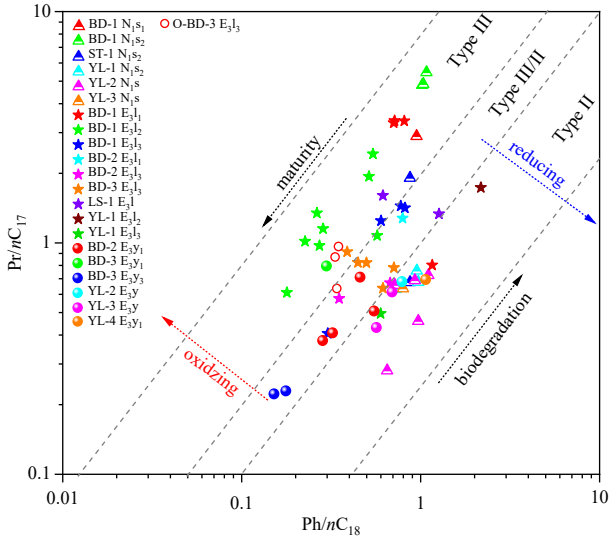

Fig. 3. Cross-plot of Ph/nC_{18} versus Pr/nC_{17} for the SRs and oils in the Qiongdongnan Basin. "O" in the legend presents oil samples.

distribution pattern with a peak at C_{23} TT, followed by C_{21} TT, and the *des*-A-oleanane was accompanied by the *des*-A-lupane (Fig. 4a); their counterparts present in model B exhibited a flat peak pattern with roughly equal C_{23} TT and C_{24} TT and had higher C_{28} TT and C_{29} TT abundances compared to other models, with a small peak of *des*-A-oleanane (Fig. 4b); the distribution pattern in model C shared a similar characteristic with model A of a unimodal distribution profile with a maximum at C_{23} TT, indicating conspicuous contributions from aquatic OM (Ahmed et al., 2012; Hakimi et al., 2021; Mohamed et al., 2018; Xu et al., 2022), but the *des*-A-lupane was undetectable in model C (Fig. 4c); and in model D these compounds were dominated by *des*-A-oleanane, with the C_{24} TeT content significantly higher than that of C_{26} TT, and the relative abundances of C_{21} TT, C_{23} TT and C_{24} TeT were very similar (Fig. 4d). Model C was dominant in all analysed samples. High abundances of C_{19} TT and C_{24} TeT relative to C_{23} TT are indicative of significant OM contributions from higher plants (Ding et al., 2022; Preston and Edwards, 2000). The source-related ratios of $C_{19}/(C_{19}+C_{23})$ TT in all 54 rock samples ranged from 0.02 to 0.77 (with an average of 0.19), one-ninth of which in the E_3l_1 and N_1s_2 strata exhibited higher C_{19} TT contents with $C_{19}/(C_{19}+C_{23})$ TT ratios of 0.57–0.77, indicating significant inputs from terrigenous OM in these rock samples. While the C_{24} TeT/C_{23} TT ratios exhibited wide-ranging values of 0.10–3.54, with an average of 0.66, one in six samples had a value larger than 1, and these samples were also representative of E_3l-N_1s. In contrast, the C_{23}/C_{21} TT ratios in the E_3y SRs range from 1.33 to 2.61, with an average of 1.95, and the ratios in the E_3l and N_1s SRs were 0.82–2.40 (average of 1.54) and 0.93–2.25 (average of 1.64), respectively.

The distribution of hopanes in the CQB reflected a general range of C_{27}–C_{35} hopanes, with C_{29}/C_{30} $\alpha\beta$ hopane ratios<1, and homohopanes with S and R epimers decreasing steadily from C_{31} to C_{35} (Fig. 4). Nevertheless, the specific distributions were diverse among these four models; e.g., model A and model C had the same characteristics of Ts/Tm ratios<1, low C_{29}Ts/C_{29} $\alpha\beta$ hopane values, and low oleanane, with the peak at C_{30} $\alpha\beta$ hopane; model B corresponded to low C_{29} $\alpha\beta$ hopane but with higher C_{29}Ts/C_{29} $\alpha\beta$ hopane ratios, moderate oleanane abundances, and Ts/Tm ratios>1, and model B exhibited higher gammacerane (IX) abundances than the other models; model D was characterized by Ts/Tm ratios>1, moderate C_{29} $\alpha\beta$ hopane and higher oleanane than C_{30} $\alpha\beta$ hopane.

The Ts/(Ts+Tm) ratios in lower Oligocene-lower Miocene rock extracts ranged from 0.07 to 0.68, among which 18.5% of samples from the E_3y-E_3l strata had values larger than 0.5, indicating relatively mature SRs. The C_{29} Ts/C_{29} $\alpha\beta$ hopane ratios ranged from 0.06 to 0.81, with an average of 0.32. The C_{29} $\alpha\beta/(\beta\alpha+\alpha\beta)$ hopane and C_{30} $\alpha\beta/(\beta\alpha+\alpha\beta)$ hopane ratios exhibited similar ranges of 0.54–0.94 (average of 0.81) and 0.47–0.89 (average of 0.79), respectively. In the E_3y SRs, the oleanane index (oleanane/C_{30} $\alpha\beta$ hopane) and gammacerane index (gammacerane/C_{30} $\alpha\beta$ hopane) values ranged from 0.04 to 1.40 and 0.11 to 0.23, respectively; in the E_3l stratum, these two ratios were in the ranges of 0.04–1.21 and 0.04–0.31, respectively; and in the N_1s stratum, the counterparts had ranges of 0.03–1.07 and 0.04–0.23, respectively. The differences among strata seemed to reflect diverse depositional environments. The relative abundances of *des*-A-oleanane and taraxerane versus C_{30} $\alpha\beta$ hopane were subtle in the SRs derived from E_3y-N_1s, with *des*-A-oleanane/C_{30} $\alpha\beta$ hopane and taraxerane/C_{30} $\alpha\beta$ hopane ratios ranging from 0.006–0.172 and 0.008–0.149, respectively. The angiosperm-related indicator of (O+DAO+Ta)/C_{30} H ranged from 0.07 to 1.62

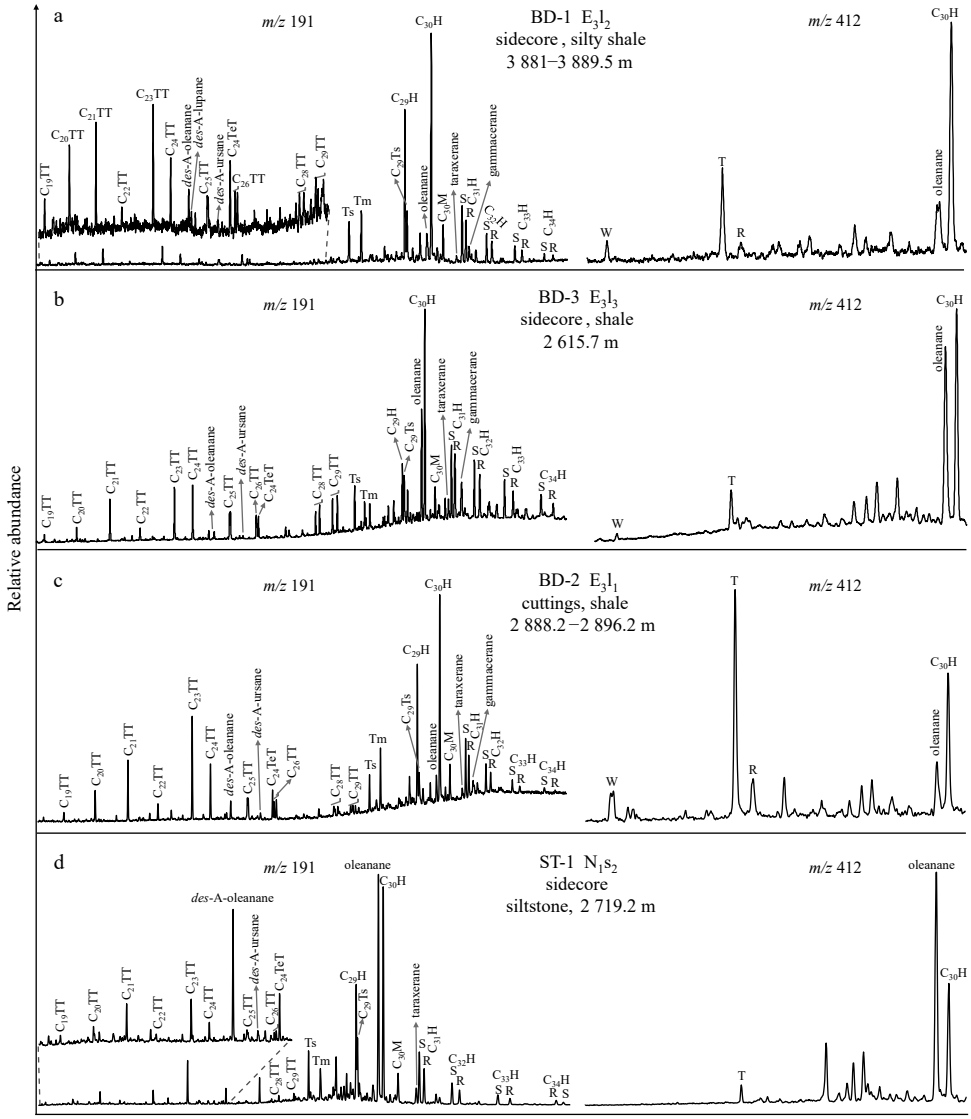

Fig. 4. Partial *m/z* 191 (left) and 412 (right) mass chromatograms of the aliphatic fractions illustrating four different distribution patterns of terpanes and bicadinanes in the rock extracts from the Qiongdongnan Basin. In *m/z* 191, TT: tricyclic teranes; TeT: tetracyclic teranes; peak distributions assign hopane stereochemistry at C-22 (S and R); Ts: 18α(H),22,29,30-trisnorneohopane; Tm: 17α(H),22,29,30-trisnorhopane; C_{29}Ts: 18α(H)-30-norneohopane; C_x, *x*: carbon number; H: 17α(H)-hopane; M: 17β(H) moretane. In *m/z* 412, W: cis-cis-trans-bicadinane; T: trans-trans-trans-bicadinane; R: bicadinane.

(with an average of 0.27) in the E_3y SRs in this study, from 0.06 to 1.47 (average of 0.42) in the E_3l SRs and from 0.06 to 1.32 (average of 0.49) in N_1s. The values of this index in the E_3l and N_1s strata were slightly higher than those in the underlying E_3y stratum, which was consistent with the characteristics illustrated by the *n*-alkanes and isoprenoids described in Section 3.1. The C_{31} 22S/(22S+22R) homohopane ratio can be used as a maturity indicator; this value very specifically denotes OM input before the mid-oil-generation window (Peters et al., 2005), and in all analysed samples, this ratio ranged from 0.31 to 0.60. Of the analysed samples, 26% reached equilibrium values of 0.57–0.62.

C_{30} bicadinane isomers varied accordingly among the four models shown in the *m/z* 412 mass chromatograms in Fig. 4. The isomers W (X) and bicadinane R were inconspicuous relative to the isomer T (XI). The isomer T was remarkably abundant in model C but had a relatively minor abundance in model D and a moderate content in model A. The (W+T)/C_{30} H ratios ranged from 0.004 to 0.167 (average of 0.038) in the E_3y SRs and were obviously lower than those measured in E_3l (0.001–0.591, average of 0.089) and N_1s (0.004–0.419, average of 0.081). *Dipterocarpaceae* has been reported to have flourished from 24.9 Ma in the late Oligocene and before declining in the early Miocene (Ding et al., 2021).

3.3 *Steranes*

The distributions of regular C_{27}, C_{28} and C_{29} $\alpha\alpha\alpha$ 20R steranes (XII), pregnanes, and partial diasteranes predominantly presented four patterns corresponding to four OM composition models, as illustrated in the *m/z* 217 mass chromatograms (Fig. 5). The distribution of C_{20}, C_{21} and C_{22} pregnanes was in a unimodal pattern with a peak at C_{21} pregnane, and regular steranes dominated over pregnanes and C_{27} diasteranes in most of the analysed samples; however, diasterane dominance was exhibited in model B, as represented by the BD-3-2 615.7 m sidecore shale (E_3l_3), and the C_{27} $\alpha\alpha\alpha$ 20R sterane showed a slight advantage over the C_{29} $\alpha\alpha\alpha$ 20R sterane (Fig. 5b), indicating its sediments under a

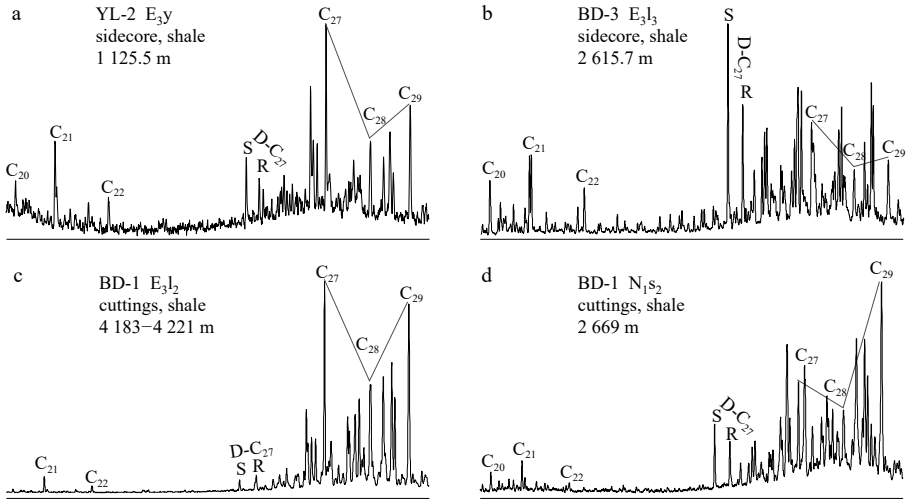

Fig. 5. Partial *m/z* 217 mass chromatograms showing the sterane and diasterane distributions in the rock extracts from the Qiongdongnan Basin. C_{20}: norpregnane; C_{21}: pregnane; C_{22}: homopregnane; D-C_{27} S: 13β(H), 17α(H)-C_{27} diasterane 20S; D-C_{27} R: 13β(H), 17α(H)-C_{27} diasterane 20R; C_{27}: C_{27} $\alpha\alpha\alpha$ 20R sterane; C_{28}: C_{28} $\alpha\alpha\alpha$ 20R sterane; C_{29}: C_{29} $\alpha\alpha\alpha$ 20R sterane.

more saline water environment and in a higher stage of maturity compared to other models. The relative contents of the C_{27}–C_{28}–C_{29} $\alpha\alpha\alpha$ 20R steranes can be used to ascertain the types of parent materials, among which C_{27} $\alpha\alpha\alpha$ 20R sterane is indicative of algae-derived OM, while C_{29} $\alpha\alpha\alpha$ 20R sterane is typical of higher plant-derived OM (Peters et al., 2005). The distributions of C_{27}, C_{28}, and C_{29} $\alpha\alpha\alpha$ 20R steranes were present with "L" "V" and "anti-L" shapes in model A, model C and model D, respectively (Figs 5a, c, d), suggesting the dissimilarity of the respective contributions from aquatic-dominant, mixed OM and terrestrial-dominant OM. The C_{27}/C_{29} $\alpha\alpha\alpha$ 20R steranes ratios in the N_1s SRs ranged from 0.31 to 1.63, and 4 out of 15 samples had ratios larger than 1.0, suggesting more terrigenous OM input than aquatic organism OM input in most samples. Accordingly, the C_{27}/C_{29} $\alpha\alpha\alpha$ 20R steranes ratios in the E_3l SRs ranged from 0.56 to 1.62, and 9 out of 28 samples had ratios larger than 1.0; the ratios measured in the E_3y SRs were in the range of 0.49–1.41, and 4 out of 11 samples had ratios less than 1.0, showing high inputs from algae- or phytoplankton-derived OM. It can thus be inferred from these values measured in all analysed samples that the contribution of terrigenous plant-derived OM was incremental from the E_3y to N_1s strata.

C_{29} sterane stereoisomers are maturity-sensitive biomarkers that can be used to specifically assess the thermal maturity of OM in the immature to mature stages (Peters et al., 2005). The C_{29} 20S/(20S+20R) steranes and C_{29} $\beta\beta/(\alpha\alpha+\beta\beta)$ steranes ratios in all associated samples were below or at their corresponding equilibrium values of 0.52–0.55 and 0.67–0.71, respectively (Peters et al., 2005; Seifert and Moldowan, 1986), with respective ranges of 0.24–0.47 and 0.40–0.53 in the E_3y SRs, 0.12–0.53 and 0.11–0.60 in the E_3l SRs, and 0.05–0.47 and 0.14–0.53 in the N_1s SRs. These stereoisomer ratios suggest that these samples did not evolve beyond the oil-generation window. The maturity- and source-related indicators associated with the partially representative samples of steranes and terpanes are listed in Table 3.

3.4 *Geochemical signatures of three supplementary DST oils*

Samples of the three analysed oils were collected from three DST sample batches in Well BD-3 of the E_3l_3 stratum; these oils had previously been confirmed to originate from the E_3y SRs (Guo et al., 2021). The three DST oils shared similar geochemical characteristics; their detailed parameters are listed in Table 3. The *n*-alkane distributions ranged from C_{15} to C_{37}, with maxima at either C_{19} or C_{20}. The evident baseline fluctuations present in the *m/z* 191 and 217 mass chromatograms are due to its light oil properties; this occurrence was validated by the relatively complete but lower abundance of high carbon number of *n*-alkanes (Fig. 6 *m/z* 85) and the apparent deficiency of steranes (Fig. 6 *m/z* 217). In the *m/z* 191 mass chromatograms, C_{21} TT, C_{23} TT and C_{24} TT peaks were predominant in the TTs distributions, and pentacyclic terpanes were dominated by *des*-A-oleanane, oleanane and C_{30} $\alpha\beta$ hopane. In particular, a remarkable abundance of the T isomer was found in the analysed bicadinanes (Fig. 6 *m/z* 412), and oleanane reflected a higher abundance relative to C_{30} $\alpha\beta$ hopane (Fig. 6 *m/z* 191), indicating significant OM contributions from terrigenous higher plants, including typical Dipterocarpaceae plants.

4 Discussion

4.1 *Thermal maturity*

The twenty-seven available vitrinite reflectance (R_o) values collected in this study ranged from 0.61% to 1.15%, and all reached the oil-generation threshold of 0.5%, and 77.8% of those were within their thermally mature stage (0.7%–1.3%). R_o and burial depth exhibited a positive correlation (with a reduction in water depth) (Fig. 7a), and the R_o values of the lower Oligocene SRs (average of 0.93%) were generally higher than those of the overlying E_3l (average of 0.80%) and N_1s (average of 0.64%) strata. Consistently, the thirty-seven available T_{max} values (for the methods of R_o and T_{max} measurements, refer to Ding et al. (2021)) were in the range of 400–451°C, among which 86.5% of these values reached the low-maturity threshold of 435°C, and 71.4% of samples were in their mature stage (440–460°C). Peters et al. (2005) reported that oils and SRs with high CPI or OEP ratios (experientially, >1.2) indicate low maturity and land plant inputs, while values of ~1.0 may arise from a predominance of marine inputs and/or thermal maturation; in particular, the values less than 0.8 are specific for low-maturity oils or bitumens from carbonatite. The relative amounts of sterane and terpanes isomerization are highly related to the parent material source, depositional environment and thermal maturity of OM, i.e., the C_{30}

Table 3. Biomarker parameters of the early Oligocene-early Miocene source rocks for representative rock samples from the Qiongdongnan Basin

Sample ID and parameters	R1	R2	R3	R4	R5	R6	R7	R8	R9	R10	R11	R12	R13	R14	R15	R16	R17	R18	R19	R20	R21	O1	O2	O3
C_{max}	21&29	29	27	20&26	19	17&27	14	17&20	22	21	20	24	29	21	25	18	20	20	27	20	18&24	20	19	20
OEP	1.38	1.32	1.03	1.12	0.99	1.00	0.80	1.12	1.00	1.02	1.10	0.98	1.22	1.21	1.26	0.76	0.96	1.03	1.18	1.05	0.90	1.08	1.01	1.08
CPI_{22-32}	1.30	1.26	1.08	1.06	1.03	1.08	1.07	1.03	1.04	1.04	1.04	1.04	1.19	1.23	1.16	0.99	0.94	1.00	1.26	1.08	1.01	1.00	1.00	1.02
Pr/Ph	2.23	3.72	3.12	1.21	1.38	1.70	1.03	1.58	1.07	2.37	1.21	1.05	0.96	0.45	0.64	0.45	0.45	0.39	0.27	0.23	0.54	1.85	1.39	1.68
Pr/nC_{17}	2.89	4.82	3.30	1.07	1.41	1.28	0.67	0.38	0.78	0.79	0.22	1.33	1.91	0.68	1.73	0.50	0.69	0.68	0.64	0.43	0.69	0.87	0.63	0.96
Ph/nC_{18}	0.95	1.02	0.71	0.57	0.82	0.79	0.68	0.28	0.71	0.30	0.15	1.27	0.87	0.97	2.17	0.60	0.93	0.79	0.80	0.57	1.07	0.33	0.34	0.35
Wax index	0.80	0.43	0.62	1.20	2.13	0.81	1.49	2.84	1.49	1.55	1.76	1.29	1.02	2.86	1.54	5.43	3.05	4.72	0.97	5.87	1.44	3.19	3.94	2.28
ACL_{15-33}	25.18	26.53	25.61	23.70	22.05	22.77	21.75	21.44	23.16	23.02	22.92	22.98	25.21	22.82	23.36	20.69	22.33	21.78	25.47	22.09	23.22	22.27	22.27	22.27
TAR	2.57	6.34	4.46	1.38	0.54	0.83	0.46	0.37	0.85	0.86	0.82	0.85	3.34	0.91	1.16	0.16	0.57	0.36	6.33	0.38	0.92	0.51	0.35	0.78
ACL_{15-33}	0.34	0.57	0.57	0.14	0.19	0.11	0.07	0.09	0.12	0.30	0.04	0.10	0.21	0.05	0.19	0.11	0.06	0.05	0.04	0.05	0.06	0.34	0.29	0.32
Pr	0.95	1.05	1.44	1.80	1.70	1.65	2.40	1.44	1.29	1.33	2.61	1.97	1.13	1.57	1.82	1.46	1.62	1.69	2.22	2.11	1.81	0.73	1.03	0.82
Ph	1.03	2.40	1.59	0.55	0.35	0.29	0.42	0.27	0.41	0.40	0.33	0.75	1.12	0.35	0.63	0.32	0.34	0.29	0.63	0.42	0.39	0.28	0.18	0.28
$C_{19}/(C_{19}+C_{23})$ TT	0.45	0.35	0.46	0.35	0.38	0.38	0.52	0.49	0.63	0.43	0.55	0.48	0.54	0.35	0.30	0.42	0.45	0.42	0.19	0.20	0.55	0.68	0.69	0.68
C_{23}/C_{21} TT	0.31	0.35	0.41	0.26	0.25	0.31	0.46	0.42	0.81	0.26	0.26	0.32	0.55	0.23	0.30	0.33	0.21	0.23	0.11	0.11	0.31	0.36	0.37	0.29
C_{24} TeT/C_{23}TT	0.80	0.82	0.90	0.86	0.83	0.88	0.91	0.88	0.92	0.88	0.85	0.90	0.80	0.69	0.66	0.77	0.78	0.74	0.68	0.56	0.83	0.91	0.90	0.93
Ts/(Ts+Tm)	0.81	0.81	0.86	0.84	0.84	0.84	0.88	0.89	0.86	0.86	0.85	0.86	0.86	0.68	0.80	0.82	0.77	0.75	0.57	0.51	0.86	0.83	0.84	0.85
C_{29}Ts/C_{29} H	0.59	0.58	0.59	0.56	0.57	0.57	0.56	0.42	0.45	0.44	0.52	0.58	0.59	0.34	0.43	0.47	0.48	0.54	0.31	0.44	0.55	0.43	0.45	0.46
C_{29} H/(H+M)	0.81	0.45	0.45	0.08	0.09	0.16	0.10	0.09	0.60	1.40	0.08	0.59	1.07	0.08	0.21	0.19	0.07	0.09	0.03	0.04	0.08	1.36	1.20	1.16
C_{30} H/(H+M)	0.06	0.05	0.06	0.23	0.23	0.15	0.21	0.20	0.29	0.15	0.22	0.04	0.07	0.23	0.10	0.18	0.17	0.17	0.13	0.11	0.17	0.21	0.21	0.16
C_{31}/C_{30} H	0.52	0.60	0.53	0.34	0.37	0.51	0.40	0.59	0.78	0.25	0.47	0.49	0.49	0.57	0.38	0.58	0.55	0.49	0.51	0.60	0.47	0.47	0.48	0.47
C_{31} H 20S/(20S+20R)	0.10	0.07	0.17	0.01	0.01	0.09	0.02	0.03	0.04	0.13	0.02	0.06	0.14	0.03	0.05	0.04	0.03	0.04	0.01	0.01	0.02	0.66	0.58	0.54
O/C_{30} H	0.15	0.12	0.13	0.03	0.04	0.08	0.03	0.02	0.12	0.09	0.02	0.06	0.10	0.06	0.05	0.07	0.02	0.02	0.02	0.01	0.03	0.16	0.15	0.15
GA/C_{30} H	1.06	0.63	0.76	0.12	0.13	0.32	0.15	0.14	0.76	1.62	0.12	0.70	1.32	0.22	0.31	0.37	0.13	0.15	0.06	0.07	0.13	2.17	1.93	1.85
DAO/C_{30} H	0.022	0.008	0.137	0.006	0.008	0.181	0.017	0.020	0.014	0.167	0.004	0.007	0.117	n.d.	n.d.	n.d.	n.d.	n.d.	0.004	n.d.	n.d.	0.382	0.337	0.336
Ta/C_{30} H	0.042	0.027	0.300	0.006	0.008	0.505	0.061	0.062	0.037	0.965	0.008	0.018	0.016	n.d.	n.d.	n.d.	n.d.	n.d.	0.055	n.d.	n.d.	0.991	0.917	0.946
$(O+DAO+Ta)/C_{30}$ H	0.67	0.31	0.69	0.81	0.85	0.88	0.65	1.02	1.17	1.23	1.18	1.62	1.36	0.97	1.32	0.68	1.39	1.23	0.56	0.49	1.41	1.16	1.49	1.85
$(W+T)/C_{30}$ H	0.40	0.47	0.42	0.38	0.38	0.53	0.44	0.45	0.47	0.47	0.39	0.43	0.44	0.05	0.12	0.18	0.40	0.35	0.24	0.24	0.43	0.45	0.47	0.51
$T/\sum C_{29}$ steranes	0.34	0.35	0.48	0.39	0.40	0.47	0.43	0.51	0.58	0.53	0.40	0.35	0.53	0.28	0.31	0.32	0.49	0.48	0.14	0.46	0.53	0.54	0.57	0.57

Notes: R*x* and O*x* are sample IDs consistent with that in Table 2. For definition of each parameter see Table 1. C_{max}: maximum *n*-alkanes; n.d.: no data.

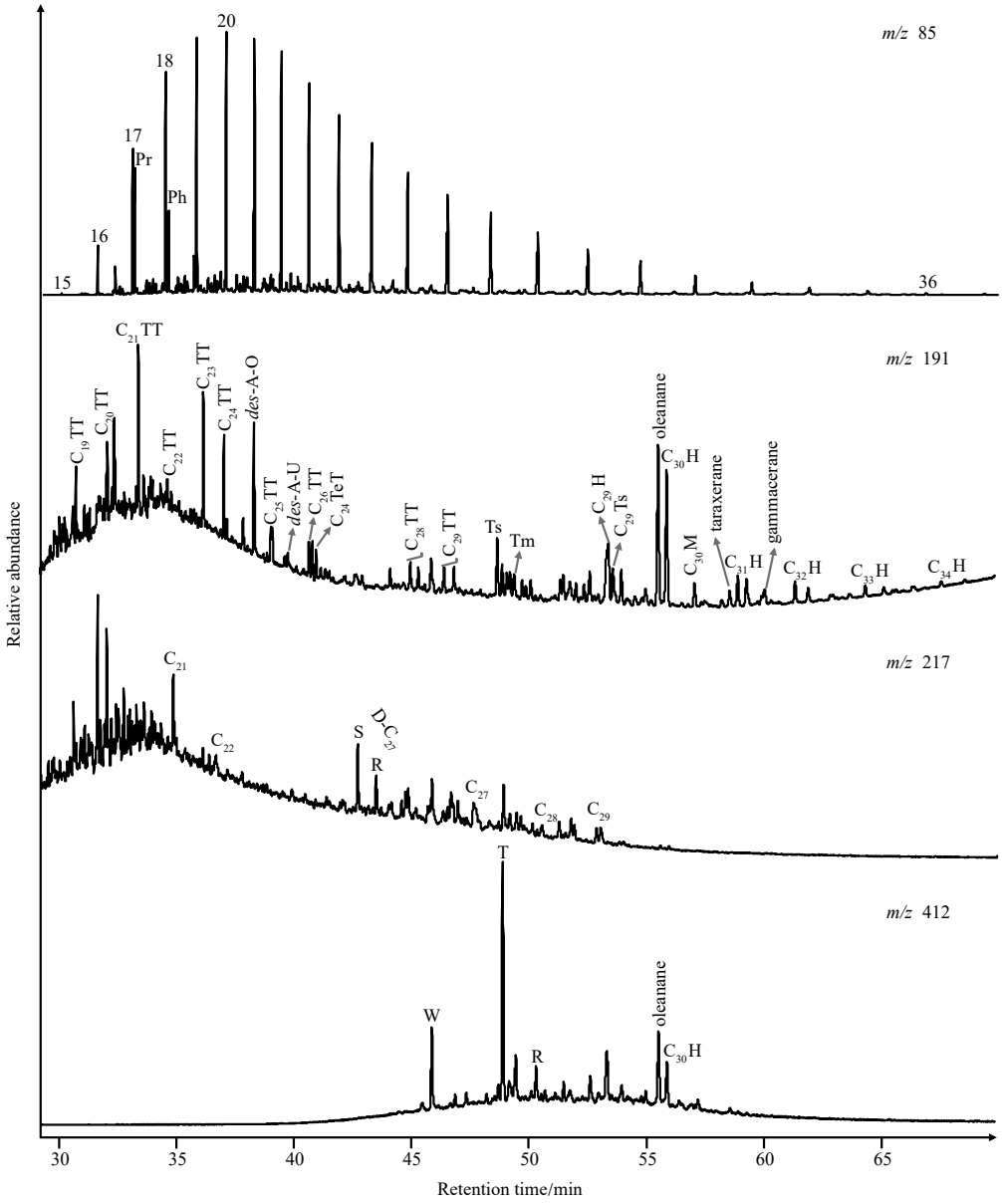

Fig. 6. *m/z* 85, 191, 217 and 412 mass chromatograms of the aliphatic hydrocarbons in drill stem test oil (2 618.1–2 680.5 m) from the lower Lingshui Formation in Well BD-3, Qiongdongnan Basin. The abbreviations refer to Figs 4 and 5.

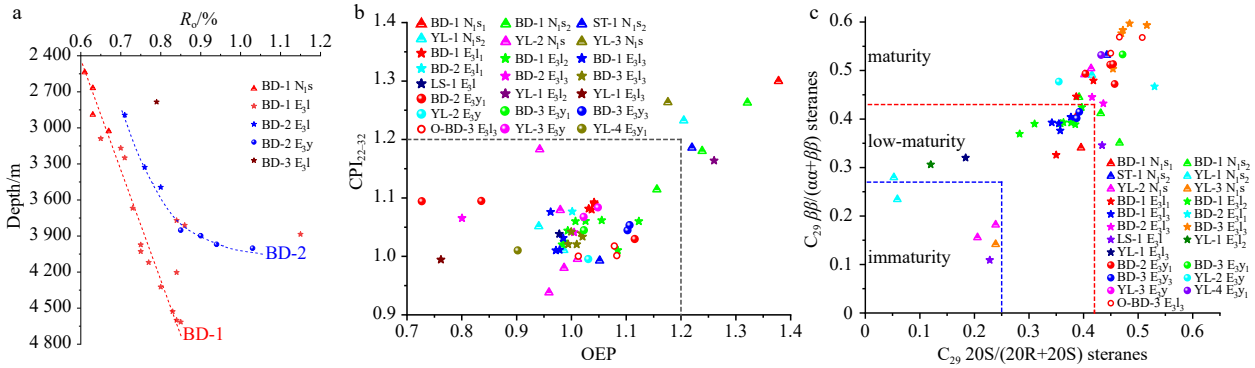

Fig. 7. Cross-plots of R_o versus depth (a), odd-to-even predominanc (OEP) versus $CPI_{22\text{-}32}$ (b), C_{29} *ααα* 20S/(20S+20R) sterane versus C_{29} 20R *ββ*/(*αα*+*ββ*) sterane (c) for samples of rock extracts and drill stem test oils. "O" in the legend presents oil samples.

αβ/(*αβ*+*βα*) hopane, C_{31} 22S/(22S+22R) homohopane, sterane stereoisomers C_{29} *ββ*/(*αα*+*ββ*) and C_{29} 20S/(20R+20S) ratios are specific for OM in the immature to mature stages (Ahmed et al., 2012; Hakimi et al., 2018; Peters et al., 2005). During burial heat-

ing, the biologically-carried R-configurations at C-20 in steroid precursors or at C-22 in hopane precursors are converted gradually to a mixture of R and S diastereomers; for example, the endpoints of the C_{29} 20S/(20R+20S) steranes are 0.52–0.55, and the equilibrium values of the C_{31}- or C_{32} 22S/(22S+22R) homohopane are 0.57–0.62. While a more stable β-configuration is formed with increasing thermal maturity when the asymmetric centre is not part of a ring, for instance, the high contents of C_{30} $\alpha\beta$ hopane relative to moretane indicate a peak hydrocarbon generation window (Ahmed et al., 2012), and the endpoints of the C_{29} $\beta\beta/(\alpha\alpha+\beta\beta)$ steranes ratios are 0.67–0.71 (Peters et al., 2005; Seifert and Moldowan, 1986). As shown in Figs 7b and c, the CPI and OEP values of most samples were between 0.9 and 1.2; correspondingly, the sterane stereoisomer ratios of C_{29} 20S/(20R+20S) steranes and C_{29} $\beta\beta/(\alpha\alpha+\beta\beta)$ steranes were mostly near or at their corresponding thermal equilibrium values, indicating that these samples were dominant in the low-maturity to mature stage, except for several Sanya SRs that exhibited either low maturity or terrigenous OM inputs. This finding can also be supported by the maturity-related biomarkers mentioned in Section 3.2, including the Ts/(Ts+Tm), C_{30} $\alpha\beta/(\beta\alpha+\alpha\beta)$ hopane and C_{31} 22S/(22S+22R) homohopane ratios. Additionally, the geochemical signatures of DST oils from Well BD-3 in E_3l_3, which originated from the E_3y SRs, can be used to verify that the lower Oligocene SRs reached the oil window due to the Ts/(Ts+Tm) (average of 0.68), C_{30} $\alpha\beta/(\beta\alpha+\alpha\beta)$ hopane (average of 0.91) and C_{31} 22S/(22S+22R) homohopane (average of 0.45) ratio indicators, as well as the standard plates shown in Figs 7b and c.

4.2 *Depositional environment*

The depositional environments of ancient sediments can be inferred using aliphatic biomarkers, e.g., the *n*-alkane distributions and relative abundances of isoprenoids (discussed in Section 3.1), the gammacerane content over C_{30} $\alpha\beta$ hopane (mentioned in Section 3.2), and the relative proportions of C_{27}-C_{29} $\alpha\alpha\alpha$ 20R steranes (described in Section 3.3).

The cross-plots of Ph/nC_{18} versus Pr/nC_{17} (Fig. 3) and C_{27}/C_{29} $\alpha\alpha\alpha$ 20R steranes versus Pr/Ph ratios (Fig. 8) constructed herein illustrate that the sediments deposited during the early Oligocene to early Miocene contained dual terrestrial and marine OM deposited under anoxic-oxic environments. The various gammacerane contents (0.04–0.31 over C_{30} $\alpha\beta$ hopane) in all samples indicated that these marine-terrigenous sediments were deposited in a transitional water environment within the study area corresponding to the incremental water depth from the early Oligocene to the early Miocene.

4.3 *Composition of OM*

Source-related biomarkers derived from aliphatic hydrocarbon fractions in sediment extracts have been widely applied to reconstruct palaeovegetation compositions over geologic time (Alexander et al., 1988; Chattopadhyay and Dutta, 2014; Ding et al., 2021; Haberer et al., 2006; Hautevelle et al., 2006; Izart et al., 2015; Jiang and George, 2018; Otto et al., 2005; Paul et al., 2015; Van Aarssen et al., 2000). For instance, a high C_{23} TT peak is indicative of abundant aquatic OM contribution (Preston and Edwards, 2000); oleanane peaks are a sign of angiosperm OM that evolved during the late Cretaceous or younger (Andrusevich et al., 1998; Grantham et al., 1983; Ten Haven and Rullkötter, 1988; Mathur, 2014; Moldowan et al., 1994; Philp and Gilbert, 1986; Rudra et al., 2017; Simoneit et al., 2020); C_{29} steranes likely stem from vascular plant-derived C_{29} sterols (Huang and Meinschein, 1979; Volkman, 2005); and the W, T isomers of bicadinanes are thought to be derived from the dammar-type resins of tropical Dipterocarpaceae plants.

Taking a series of *n*-alkane ratios into consideration, the moderate ACL values and large TAR ratio ranges measured in all samples indicated mixed OM inputs to the analysed lower Oligocene-lower Miocene SRs, while the partial presence of shorter *n*-alkane chain lengths and minor TAR values also pointed to dominant contributions from marine phytoplankton- and algal-derived OM, and the relatively high CPI and OEP values (>1.2), extremely high TAR values (up to 8.03) and long *n*-alkane chain lengths were indicative of terrestrial higher plant-dominant sources.

The general presence of angiosperm-derived biomarkers, including oleanane, *des*-A-oleanane, *des*-A-ursane, and taraxerane peaks, as well as the varying bicadinane amounts in all analysed samples, indicate the wide contributions of angiosperms such as myrtles and Dipterocarpaceae. Moreover, the extremely high oleanane amount in model C suggested angiosperm-dominant OM to its SRs. However, no explicit correlation between oleanane

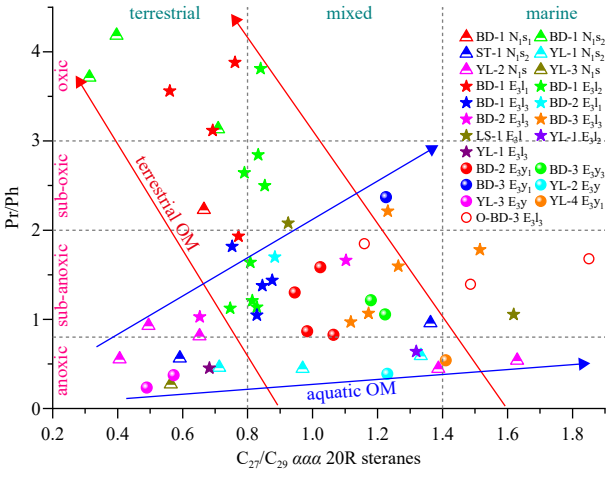

Fig. 8. Cross-plot of the C_{27}/C_{29} $\alpha\alpha\alpha$ 20R steranes versus the Pr/Ph ratio for all analyzed samples from the lower Oligocene to lower Miocene in the Qiongdongnan Basin. "O" in the legend presents oil samples. OM: organic matter.

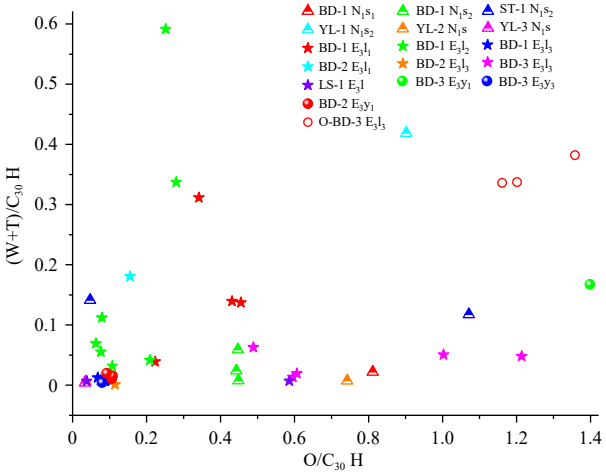

Fig. 9. Cross-plot of the O/C_{30} H versus (W+T)/C_{30} H for rock extracts and drill stem test oils. "O" in the legend presents oil samples.

and the (W+T) isomers of bicadinanes was found (Fig. 9). The (O+DAO+Ta)/C_{30} H values measured in all the samples exhibited an increase in average values from the lower Oligocene (0.27) to the upper Oligocene (0.42) and to the lower Miocene (0.49), indicating that angiosperms (e.g., myrtles) played an elevated role in palaeofloras from the early Oligocene to the early Miocene. This finding is further corroborated by the higher C_{19} TT abundances and larger C_{24} TeT/C_{23} TT values in the E_3l-N_1s sediments relative to those in the E_3y SRs. In contrast, moderate to high abundances of C_{23} TT (C_{23} TT/C_{21} TT ratios≈0.82–2.61) in the CQB SRs pointed to significant contributions from aquatic OM, and the higher values in the E_3y SRs (average of 1.95) compared to those in E_3l-N_1s strata (average of 1.57) are indicative of more contributions from aquatic OM to the E_3y sediments than to the E_3l-N_1s SRs.

Steranes are derived from sterols in algal organisms and higher land plants. Regular C_{27} steranes are generally accepted to be indicative of marine phytoplankton, zooplankton and algal sources, while regular C_{29} steranes have been regarded as features of terrestrial plants and diatoms. Moreover, significant abundances of regular C_{28} steranes are highly specific in their indication of lacustrine algal organisms (Jiang and George, 2018; Volkman, 2005). As shown in the ternary diagram displaying the relative proportions of C_{27}, C_{28}, and C_{29} *ααα* 20R steranes (Fig. 10), the positions of all available samples were intensively located in the region where suggesting mixed terrestrial and aquatic OM sources (corresponding to model C), with partial N_1s SRs dominated by terrestrial sources (corresponding to model D). The cross-plot of the C_{27}/C_{29} *ααα* 20R steranes versus the Pr/Ph ratio (Fig. 8) shows that the compounds in all the samples were characterised by mixed contribution from terrigenous and marine OM under sub-anoxic to anoxic environmental conditions. The terrestrial-dominant SRs were interpreted to be developed mainly in the Lingshui-Sanya formations and deposited in sub-oxic to oxic environments, compared to the anoxic to sub-anoxic conditions of Yacheng Formation.

The Red River has been reported to be a stable source provenance for the central Canyon in the CQB, exhibiting a large transport rate (>100 Mt/a) since the late Oligocene (Fyhn et al., 2019; Lei et al., 2019; Zhao et al., 2015); in contrast, along the north-western margin of the CQB, the deposits are dominated by the subordinate Hainan Island provenance (Fyhn et al., 2019; Li et al., 2019; Wang et al., 2016; Zhao et al., 2019). Terrigenous OM and clastic fragments were transported into this studied marginal marine environment through the source-to-sink Red River and Hainan Island systems, causing the marine-terrigenous SRs analysed herein to be specific to the transitional water environments in continental marginal basins, such as the Qiongdongnan Basin.

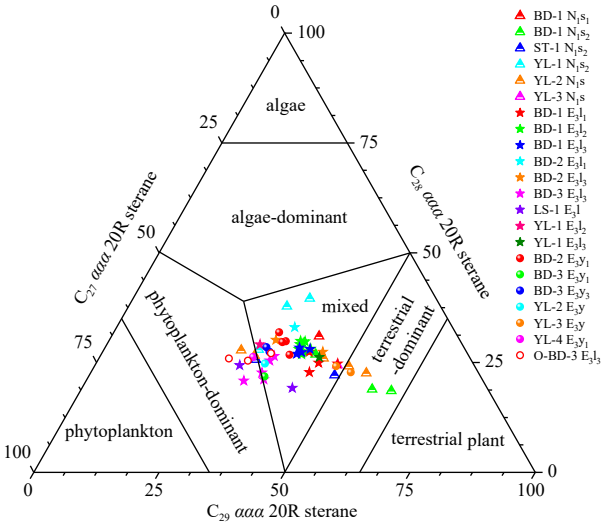

Fig. 10. Ternary diagram of the C_{27}-C_{28}-C_{29} *ααα* 20R steranes for the rock extracts and drill stem test oils in the Qiongdongnan Basin. "O" in the legend presents oil samples.

In summary, aquatic organisms and terrigenous higher plants are vital components of OM in CQB SRs. Combined with the above interpreted aliphatic biomarker signatures of early Oligocene–early Miocene SRs in the CQB, the roughly increased terrigenous OM input to ancient sediments from the E_3y stratum to the N_1s stratum was observed in this study. The exact variations in the contribution from terrestrial higher plant-derived OM during the late Oligocene–early Miocene could be visually exhibited in Well BD-1 (Fig. 11), characterized by a terrigenous OM enrichment in the E_3l_1-N_1s_2 transitional period; this finding was consistent with the indication of the bulk geochemical parameters of the SRs herein, in which the total organic carbon (TOC) and free hydrocarbons + potential hydrocarbons (S_1+S_2) (the analytical methods for TOC, S_1 and S_2, refer to Ding et al. (2021)) gradually increased during the depositional period from E_3l_3 to N_1s_2, and they were especially enriched in E_3l_1–N_1s_2 strata (Fig. 12); however, this discovery was realized on the basis of a finite dataset; nevertheless, it can also be reinforced by the idea that a prominently higher abundance of angiosperm-dominated OM was deposited in the E_3l_1-N_1s_2 strata (approximately 24.9–18.3 Ma) than in the other underlying formations (during 28.4–24.9 Ma) (Ding et al., 2021), and the discovery was further corroborated by Oligocene palynological records in the South China Sea, which indicated that the palaeoclimate gradually changed from tropical/subtropical conditions to temperate conditions after the late Oligocene (Ding et al., 2021; Wu et al., 2003).

5 Conclusions

The aliphatic hydrocarbons in the fifty-four lower Oligocene-lower Miocene rock samples and three oils from the CQB were analysed in this study to investigate their thermal maturity, depositional environments and OM sources.

(1) Maturity-sensitive indicators such as isomerisation ratios of sterane and hopanes, together with *Ro* and T_{max} values, suggest that the thermal maturity of the samples have predominantly reached the early oil-generation window but have not exceeded the peak oil windows, except for some immature Sanya Formation shales.

(2) The terrestrial-dominant SRs developed mainly in the Lingshui-Sanya formations and were deposited in sub-oxic to oxic environments compared to the anoxic to sub-anoxic conditions of the Yacheng Formation. The OM in all the samples was predominantly characterised by mixed contributions from terrigenous and marine OM under anoxic to sub-anoxic environments, suggesting a transitional aquatic environment of these terrigenous-marine SRs in the continental margin basin.

(3) Both terrestrial higher plant- and aquatic-derived OM contributed to the lower Oligocene–lower Miocene SRs in the CQB but have varying relative contributions to the OM. Four source analytical models of OM in CQB SRs were interpreted in this study. Model A to model D have increased contributions of terrigenous OM. Additionally, angiosperms played an enhancing role in palaeofloras from the early Oligocene to the early Miocene, and the bloom of terrigenous higher plants was observed during the deposition of E_3l_1 to N_1s_2 strata.

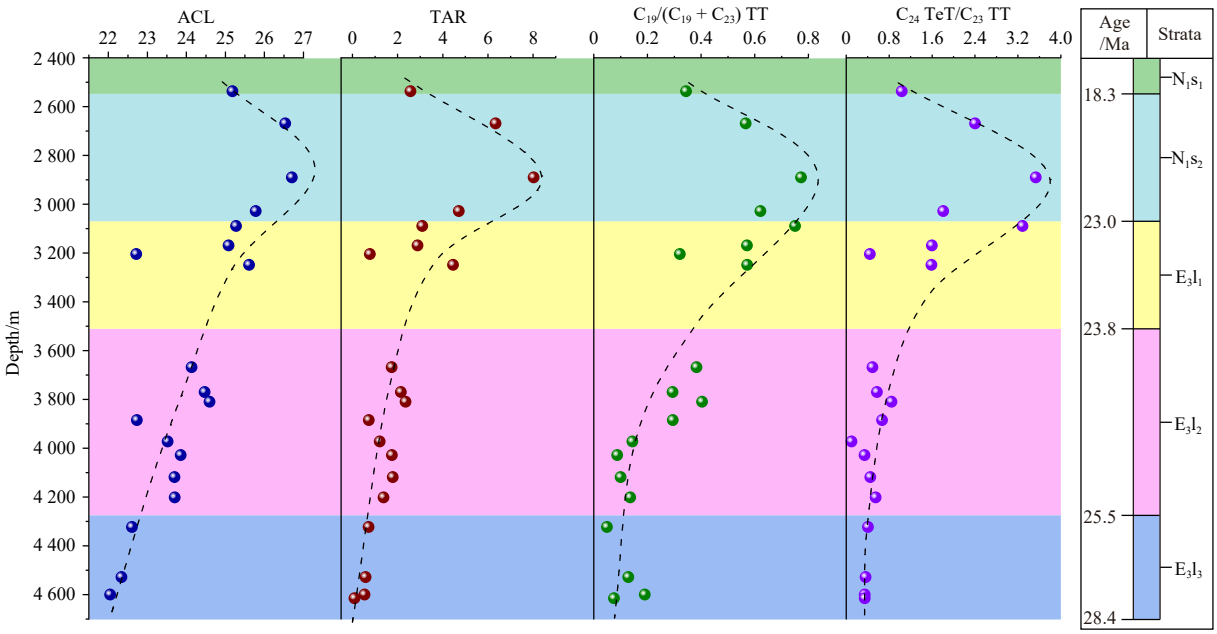

Fig. 11. Cross-plot of terrestrial-derived indicators versus depths from middle lingshui Formation to lower Sanya Formation in Well BD-1. For abbreviations, see Table 1.

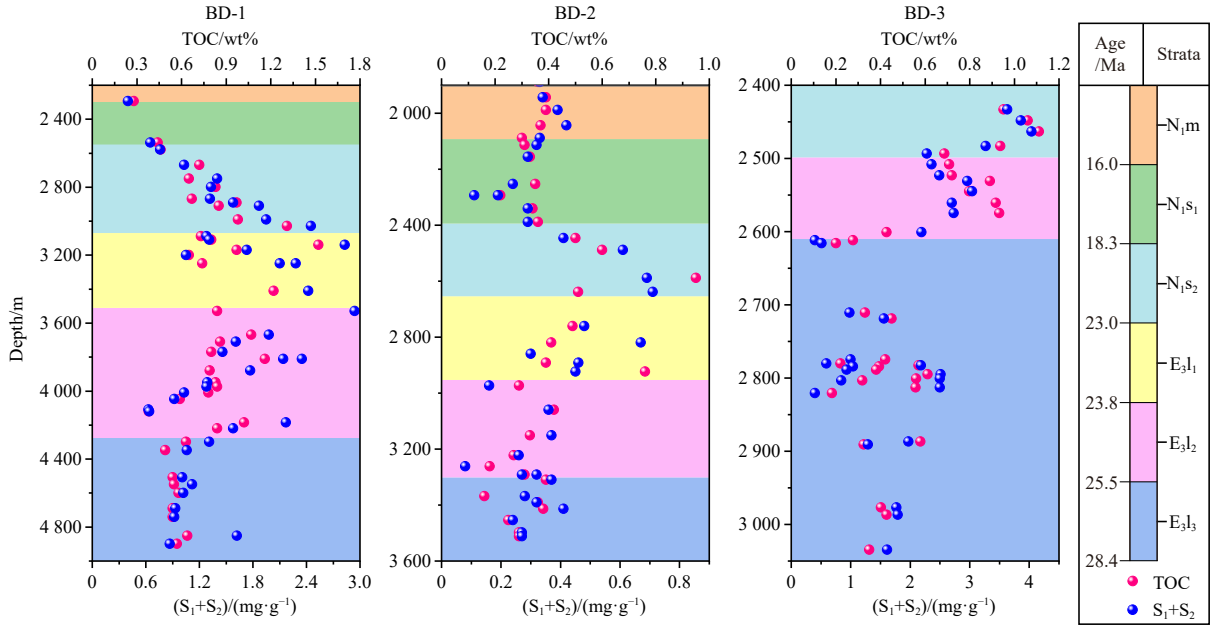

Fig. 12. Vertical variations of total organic carbon (TOC) and hydrocarbon-generation potential (S_1+S_2) of source rocks in three representative wells in the Qiongdongnan Basin.

References

Ahmed M, Volk H, Allan T, et al. 2012. Origin of oils in the eastern Papuan Basin, Papua New Guinea. Organic Geochemistry, 53: 137–152, doi: 10.1016/j.orggeochem.2012.06.002

Albrecht P, Vandenbroucke M, Mandengué M. 1976. Geochemical studies on the organic matter from the Douala Basin (Cameroon)—I. Evolution of the extractable organic matter and the formation of petroleum. Geochimica et Cosmochimica Acta, 40(7): 791–799, doi: 10.1016/0016-7037(76)90031-4

Alexander R, Larcher A V, Kagi R I, et al. 1988. The use of plant derived biomarkers for correlation of oils with source rocks in the Cooper/Eromanga Basin system, Australia. The APPEA Journal, 28(1): 310–324, doi: 10.1071/AJ87024

Alkhafaji M W. 2021. Biomarker assessment of oil biodegradation, water washing, and source rock characteristics of oil seeps from the Foothill Zone along the Tigris River, Northern Iraq. Journal of Petroleum Science and Engineering, 197: 107946, doi: 10.1016/j.petrol.2020.107946

Andrusevich V E, Engel M H, Zumberge J E, et al. 1998. Secular, episodic changes in stable carbon isotope composition of crude oils. Chemical Geology, 152(1–2): 59–72

Blocho R M, Smith R W, Noll M R. 2021. Analyses of depositional environments of the Marcellus formation in New York using biomarker and trace metal proxies. Journal of Petroleum Exploration and Production Technology, 11(8): 3163–3175, doi: 10.1007/s13202-021-01237-8

Bourbonniere R A, Meyers P A. 1996. Sedimentary geolipid records of historical changes in the watersheds and productivities of

Lakes Ontario and Erie. Limnology and Oceanography, 41(2): 352–359, doi: 10.4319/lo.1996.41.2.0352
Cao Ying, Li Chunfeng, Yao Yongjian. 2017. Thermal subsidence and sedimentary processes in the South China Sea Basin. Marine Geology, 394: 30–38, doi: 10.1016/j.margeo.2017.07.022
Chattopadhyay A, Dutta S. 2014. Higher plant biomarker signatures of early Eocene sediments of North Eastern India. Marine and Petroleum Geology, 57: 51–67, doi: 10.1016/j.marpetgeo.2014.04.004
Didyk B M, Simoneit B R T, Brassell S C, et al. 1978. Organic geochemical indicators of palaeoenvironmental conditions of sedimentation. Nature, 272(5650): 216–222, doi: 10.1038/272216a0
Ding Wenjing, Hou Dujie, Gan Jun, et al. 2021. Palaeovegetation variation in response to the late Oligocene–early Miocene East Asian summer monsoon in the Ying-Qiong Basin, South China Sea. Palaeogeography, Palaeoclimatology, Palaeoecology, 567: 110205
Ding Wenjing, Hou Dujie, Gan Jun, et al. 2022. Sedimentary geochemical records of late Miocene-early Pliocene palaeovegetation and palaeoclimate evolution in the Ying-Qiong Basin, South China Sea. Marine Geology, 445: 106750, doi: 10.1016/j.margeo.2022.106750
Ding Wenjing, Hou Dujie, Zhang Weiwei, et al. 2018. A new genetic type of natural gases and origin analysis in northern Songnan-Baodao Sag, Qiongdongnan Basin, South China Sea. Journal of Natural Gas Science and Engineering, 50: 384–398, doi: 10.1016/j.jngse.2017.12.003
Eglinton G, Hamilton R J. 1967. Leaf Epicuticular Waxes: The waxy outer surfaces of most plants display a wide diversity of fine structure and chemical constituents. Science, 156(3780): 1322–1335, doi: 10.1126/science.156.3780.1322
Fan Caiwei, Xu Changgui, Xu Jie. 2021. Genesis and characteristics of miocene deep-water clastic rocks in Yinggehai and Qiongdongnan Basins, northern South China Sea. Acta Geologica Sinica (English Edition), 95(1): 153–166, doi: 10.1111/1755-6724.14637
Fazeelat T, Asif M, Jalees M I, et al. 2011. Source correlation between biodegraded oil seeps and a commercial crude oil from the Punjab Basin, Pakistan. Journal of Petroleum Science and Engineering, 77(1): 1–9, doi: 10.1016/j.petrol.2011.01.003
Fyhn M B W, Thomsen T B, Keulen N, et al. 2019. Detrital zircon ages and heavy mineral composition along the Gulf of Tonkin—Implication for sand provenance in the Yinggehai-Song Hong and Qiongdongnan basins. Marine and Petroleum Geology, 101: 162–179, doi: 10.1016/j.marpetgeo.2018.11.051
Galarraga F, Urbani F, Escobar M, et al. 2010. Main factors controlling the compositional variability of seepage oils from Trujillo state, western Venezuela. Journal of Petroleum Geology, 33(3): 255–267, doi: 10.1111/j.1747-5457.2010.00477.x
Gao Gang, Zhang Gongcheng, Chen Guo, et al. 2018. Geochemistry of borehole cutting shale and natural gas accumulation in the deepwater area of the Zhujiang River Mouth-Qiongdongnan Basin in the northern South China Sea. Acta Oceanologica Sinica, 37(2): 44–53, doi: 10.1007/s13131-018-1151-2
Grantham P J, Posthuma J, Baak A. 1983. Triterpanes in a number of Far-Eastern crude oils. In: Bjory M, Albrecht C, eds. Advances in Organic Geochemistry 1981: International Conference Proceedings. Chichester: Blackwell, 710–724
Guo Shusheng, Liao Gaolong, Liang Hao, et al. 2021. Major breakthrough and significance of deep-water gas exploration in Well BD21 in Qiongdongnan Basin. China Petroleum Exploration, 26(5): 49–59
Haberer R M, Mangelsdorf K, Wilkes H, et al. 2006. Occurrence and palaeoenvironmental significance of aromatic hydrocarbon biomarkers in Oligocene sediments from the Mallik 5L-38 Gas Hydrate Production Research Well (Canada). Organic Geochemistry, 37(5): 519–538, doi: 10.1016/j.orggeochem.2006.01.004
Hakimi M H, Abdullah E S, Ebiad M A, et al. 2021. Early mature sulfur-rich oils from the central gulf of Suez province: bulk property and geochemical investigations of maltene and asphaltene show source related-type. Arabian Journal of Geosciences, 14(12): 1119, doi: 10.1007/s12517-021-07280-3
Hakimi M H, Mohialdeen I M J, Al Ahmed A A, et al. 2018. Thermal modeling and hydrocarbon generation of the late Jurassic–early Cretaceous Chia Gara Formation in Iraqi Kurdistan region, northern Zagros Fold Belt. Egyptian Journal of Petroleum, 27(4): 701–713, doi: 10.1016/j.ejpe.2017.10.007
Hautevelle Y, Michels R, Malartre F, et al. 2006. Vascular plant biomarkers as proxies for palaeoflora and palaeoclimatic changes at the Dogger/Malm transition of the Paris Basin (France). Organic Geochemistry, 37(5): 610–625, doi: 10.1016/j.orggeochem.2005.12.010
Hoş-Çebi F. 2017. Organic geochemical characteristics and paleoclimate conditions of the Miocene coals at the Çan-Durali (Çanakkale). Journal of African Earth Sciences, 129: 117–135, doi: 10.1016/j.jafrearsci.2016.12.003
Huang Heting, Huang Baojia, Huang Yiwen, et al. 2017. Condensate origin and hydrocarbon accumulation mechanism of the deepwater giant gas field in western South China Sea: A case study of Lingshui 17–2 gas field in Qiongdongnan Basin. Petroleum Exploration and Development, 44(3): 409–417, doi: 10.1016/S1876-3804(17)30047-2
Huang Baojia, Li Li, Huang Heting. 2012. Origin and accumulation mechanism of shallow gases in the North Baodao Slope, Qiongdongnan Basin, South China Sea. Petroleum Exploration and Development, 39(5): 567–573, doi: 10.1016/S1876-3804(12)60077-9
Huang Wen-Yen, Meinschein W G. 1979. Sterols as ecological indicators. Geochimica et Cosmochimica Acta, 43(5): 739–745, doi: 10.1016/0016-7037(79)90257-6
Huang Baojia, Tian Hui, Li Xushen, et al. 2016. Geochemistry, origin and accumulation of natural gases in the deepwater area of the Qiongdongnan Basin, South China Sea. Marine and Petroleum Geology, 72: 254–267, doi: 10.1016/j.marpetgeo.2016.02.007
Huang Baojia, Xiao Xianming, Li Xuxuan. 2003. Geochemistry and origins of natural gases in the Yinggehai and Qiongdongnan basins, offshore South China Sea. Organic Geochemistry, 34(7): 1009–1025, doi: 10.1016/S0146-6380(03)00036-6
Izart A, Suarez-Ruiz I, Bailey J. 2015. Paleoclimate reconstruction from petrography and biomarker geochemistry from Permian humic coals in Sydney Coal Basin (Australia). International Journal of Coal Geology, 138: 145–157, doi: 10.1016/j.coal.2014.12.009
Jeng W L. 2006. Higher plant *n*-alkane average chain length as an indicator of petrogenic hydrocarbon contamination in marine sediments. Marine Chemistry, 102(3–4): 242–251
Jiang Lian, Ding Wenjing, George S C. 2020. Late Cretaceous–Paleogene palaeoclimate reconstruction of the Gippsland Basin, SE Australia. Palaeogeography, Palaeoclimatology, Palaeoecology, 556: 109885
Jiang Lian, George S C. 2018. Biomarker signatures of Upper Cretaceous Latrobe Group hydrocarbon source rocks, Gippsland Basin, Australia: Distribution and palaeoenvironment significance of aliphatic hydrocarbons. International Journal of Coal Geology, 196: 29–42, doi: 10.1016/j.coal.2018.06.025
Jiang Lian, George S C. 2019. Biomarker signatures of Upper Cretaceous Latrobe Group petroleum source rocks, Gippsland Basin, Australia: Distribution and geological significance of aromatic hydrocarbons. Organic Geochemistry, 138: 103905, doi: 10.1016/j.orggeochem.2019.103905
Kennicutt M C, Barker C, Brooks J M, et al. 1987. Selected organic-matter source indicators in the orinoco, Nile and Changjiang deltas. Organic Geochemistry, 11(1): 41–51, doi: 10.1016/0146-6380(87)90050-7
La Croix A D, He Jianhua, Bianchi V, et al. 2020. Early Jurassic palaeoenvironments in the Surat Basin, Australia—marine incursion into eastern Gondwana. Sedimentology, 67(1): 457–485, doi: 10.1111/sed.12649
Lai Hongfei, Fang Yunxin, Kuang Zenggui, et al. 2021. Geochemistry, origin and accumulation of natural gas hydrates in the Qiongdongnan Basin, South China Sea: implications from site GMGS5-W08. Marine and Petroleum Geology, 123: 104774, doi:

10.1016/j.marpetgeo.2020.104774
Large D J, Gize A P. 1996. Pristane/phytane ratios in the mineralized Kupferschiefer of the Fore-Sudetic Monocline, southwest Poland. Ore Geology Reviews, 11(1–3): 89–103
Lei Chao, Clift P D, Ren Jianye, et al. 2019. A rapid shift in the sediment routing system of lower-upper Oligocene strata in the Qiongdongnnan Basin (Xisha Trough), Northwest South China Sea. Marine and Petroleum Geology, 104: 249–258, doi: 10.1016/j.marpetgeo.2019.03.012
Li Chao, Lyu Chengfu, Chen Guojun, et al. 2019. Zircon U-Pb ages and REE composition constraints on the provenance of the continental slope-parallel submarine fan, western Qiongdongnan Basin, northern margin of the South China Sea. Marine and Petroleum Geology, 102: 350–362, doi: 10.1016/j.marpetgeo.2018.12.046
Li Wenhao, Zhang Zhihuan. 2017. Paleoenvironment and its control of the formation of oligocene marine source rocks in the deepwater area of the northern South China Sea. Energy & Fuels, 31(10): 10598–10611
Li Hangyu, Zhang Ming, Lau H C, et al. 2020. China's deepwater development: subsurface challenges and opportunities. Journal of Petroleum Science and Engineering, 195: 107761, doi: 10.1016/j.petrol.2020.107761
Li Wenhao, Zhang Zhihuan, Li Youchuan, et al. 2012. New perspective of Miocene marine hydrocarbon source rocks in deep-water area in Qiongdongnan Basin of northern South China Sea. Acta Oceanologica Sinica, 31(5): 107–114, doi: 10.1007/s13131-012-0241-9
Li Wenhao, Zhang Zhihuan, Li Youchuan, et al. 2013. The main controlling factors and developmental models of Oligocene source rocks in the Qiongdongnan Basin, northern South China Sea. Petroleum Science, 10(2): 161–170, doi: 10.1007/s12182-013-0263-8
Liu Zhen, Sun Zhipeng, Wang Zisong, et al. 2016a. Evaluation of abundant hydrocarbon-generation depressions in the deepwater area of Qiongdongnan Basin, South China Sea. Acta Oceanologica Sinica, 35(2): 137–144, doi: 10.1007/s13131-015-0784-7
Liu Zhifei, Zhao Yulong, Colin C, et al. 2016b. Source-to-sink transport processes of fluvial sediments in the South China Sea. Earth-Science Reviews, 153: 238–273, doi: 10.1016/j.earscirev.2015.08.005
Mathur N. 2014. Tertiary oils from Upper Assam Basin, India: a geochemical study using terrigenous biomarkers. Organic Geochemistry, 76: 9–25, doi: 10.1016/j.orggeochem.2014.07.007
Miao Yufa, Warny S, Clift P D, et al. 2018. Climatic or tectonic control on organic matter deposition in the South China Sea? A lesson learned from a comprehensive Neogene palynological study of IODP Site U1433. International Journal of Coal Geology, 190: 166–177, doi: 10.1016/j.coal.2017.10.003
Mohamed N S, El Nady M M, Sharaf L M. 2018. Evaluation of possible source rocks and extracts characteristics from Safir-1x well, North Western Desert, Egypt. Petroleum Science and Technology, 36(16): 1235–1241, doi: 10.1080/10916466.2018.1465974
Moldowan J M, Dahl J, Huizinga B J, et al. 1994. The molecular fossil record of oleanane and its relation to angiosperms. Science, 265(5173): 768–771, doi: 10.1126/science.265.5173.768
Murray A P, Sosrowidjojo I B, Alexander R, et al. 1997. Oleananes in oils and sediments: Evidence of marine influence during early diagenesis?. Geochimica et Cosmochimica Acta, 61(6): 1261–1276
Nytoft H P, Kildahl-Andersen G, Samuel O J. 2010. Rearranged oleananes: Structural identification and distribution in a worldwide set of late Cretaceous/Tertiary oils. Organic Geochemistry, 41(10): 1104–1118, doi: 10.1016/j.orggeochem.2010.06.008
Otto A, Simoneit B R T, Rember W C. 2005. Conifer and angiosperm biomarkers in clay sediments and fossil plants from the Miocene Clarkia Formation, Idaho, USA. Organic Geochemistry, 36(6): 907–922, doi: 10.1016/j.orggeochem.2004.12.004
Ourisson G, Albrecht P, Rohmer M. 1979. The hopanoids: palaeochemistry and biochemistry of a group of natural products. Pure and Applied Chemistry, 51(4): 709–729, doi: 10.1351/pac197951040709
Ourisson G, Albrecht P, Rohmer M. 1982. Predictive microbial biochemistry—from molecular fossils to procaryotic membranes. Trends in Biochemical Sciences, 7(7): 236–239, doi: 10.1016/0968-0004(82)90028-7
Paul S, Sharma J, Singh B D, et al. 2015. Early Eocene equatorial vegetation and depositional environment: Biomarker and palynological evidences from a lignite-bearing sequence of Cambay Basin, western India. International Journal of Coal Geology, 149: 77–92, doi: 10.1016/j.coal.2015.06.017
Peters K E, Fraser T H, Amris W, et al. 1999. Geochemistry of crude oils from eastern Indonesia. AAPG Bulletin, 83(12): 1927–1942
Peters K E, Walters C C, Moldowan J M. 2005. The Biomarker Guide. Cambridge: Cambridge University Press
Philp R P, Gilbert T D. 1986. Biomarker distributions in australian oils predominantly derived from terrigenous source material. Organic Geochemistry, 10(1–3): 73–84
Preston J C, Edwards D. 2000. The petroleum geochemistry of oils and source rocks from the northern Bonaparte Basin, offshore northern Australia. The APPEA Journal, 40(1): 257–282, doi: 10.1071/AJ99014
Ren Jianye, Lei Chao, Wang Shan, et al. 2011. Tectonic stratigraphic framework of Yinggehai-Qiongdongnan Basins and its implication for tectonic province division in South China Sea. Chinese Journal of Geophysics, 54(12): 3303–3314
Ren Jinfeng, Wang Hua, Sun Ming, et al. 2014. Sequence stratigraphy and sedimentary facies of lower Oligocene Yacheng Formation in deepwater area of Qiongdongnan Basin, northern South China Sea: implications for coal-bearing source rocks. Journal of Earth Science, 25(5): 871–883, doi: 10.1007/s12583-014-0479-6
Ren Jinfeng, Zhang Yingzhao, Wang Hua, et al. 2015. Identification methods of coal-bearing source rocks for Yacheng Formation in the western deepwater area of South China Sea. Acta Oceanologica Sinica, 34(4): 19–31, doi: 10.1007/s13131-015-0647-2
Rudra A, Dutta S, Raju S V. 2017. The Paleogene vegetation and petroleum system in the tropics: A biomarker approach. Marine and Petroleum Geology, 86: 38–51, doi: 10.1016/j.marpetgeo.2017.05.008
Samad S K, Mishra D K, Mathews R P, et al. 2020. Geochemical attributes for source rock and palaeoclimatic reconstruction of the Auranga Basin, India. Journal of Petroleum Science and Engineering, 185: 106665, doi: 10.1016/j.petrol.2019.106665
Seifert W K, Moldowan M J. 1978. Applications of steranes, terpanes and monoaromatics to the maturation, migration and source of crude oils. Geochimica et Cosmochimica Acta, 42(1): 77–95, doi: 10.1016/0016-7037(78)90219-3
Seifert W K, Moldowan J M. 1986. Use of biological markers in petroleum exploration. In: Johns R B, ed. Methods in Geochemistry and Geophysics. Msterdam: Elsevier, 261–290
Simoneit B R T, Oros D R, Karwowski Ł, et al. 2020. Terpenoid biomarkers of ambers from Miocene tropical paleoenvironments in Borneo and of their potential extant plant sources. International Journal of Coal Geology, 221: 103430, doi: 10.1016/j.coal.2020.103430
Su Ao, Chen Honghan, Chen Xu, et al. 2018. New insight into origin, accumulation and escape of natural gas in the Songdong and Baodao regions in the eastern Qiongdongnan Basin, South China Sea. Journal of Natural Gas Science and Engineering, 52: 467–483, doi: 10.1016/j.jngse.2018.01.026
Su Ao, Chen Honghan, He Cong, et al. 2017. Complex accumulation and leakage of YC21–1 gas bearing structure in Yanan Sag, Qiongdongnan Basin, South China Sea. Marine and Petroleum Geology, 88: 798–813, doi: 10.1016/j.marpetgeo.2017.09.020
Su Long, Zheng Jianjing, Chen Guojun, et al. 2012. The upper limit of maturity of natural gas generation and its implication for the Yacheng Formation in the Qiongdongnan Basin, China. Journal of Asian Earth Sciences, 54–55: 203–213
Tamburini F, Adatte T, Föllmi K, et al. 2003. Investigating the history of East Asian monsoon and climate during the last glacial-interglacial period (0–140 000 years): Mineralogy and geochemistry

of ODP Sites 1143 and 1144, South China Sea. Marine Geology, 201(1–3): 147–168

Ten Haven H L, De Leeuw J W, Schenck P A. 1985. Organic geochemical studies of a Messinian evaporitic basin, northern Apennines (Italy) I: Hydrocarbon biological markers for a hypersaline environment. Geochimica et Cosmochimica Acta, 49(10): 2181–2191, doi: 10.1016/0016-7037(85)90075-4

Ten Haven H L, Rullkötter J. 1988. The diagenetic fate of taraxer-14-ene and oleanene isomers. Geochimica et Cosmochimica Acta, 52(10): 2543–2548, doi: 10.1016/0016-7037(88)90312-2

Ten Haven H L, Rullkötter J, De Leeuw J W, et al. 1988. Pristane/phytane ratio as environmental indicator. Nature, 333(6174): 604–604

Van Aarssen B G K, Alexander R, Kagi R I. 2000. Higher plant biomarkers reflect palaeovegetation changes during Jurassic times. Geochimica et Cosmochimica Acta, 64(8): 1417–1424, doi: 10.1016/S0016-7037(99)00432-9

Van Aarssen B G K, Hessels J K C, Abbink O A, et al. 1992. The occurrence of polycyclic sesqui-, tri-, and oligoterpenoids derived from a resinous polymeric cadinene in crude oils from Southeast Asia. Geochimica et Cosmochimica Acta, 56(3): 1231–1246, doi: 10.1016/0016-7037(92)90059-R

Volkman J K. 2005. Sterols and other triterpenoids: Source specificity and evolution of biosynthetic pathways. Organic Geochemistry, 36(2): 139–159, doi: 10.1016/j.orggeochem.2004.06.013

Vuković N, Životić D, Filho J G M, et al. 2016. The assessment of maturation changes of humic coal organic matter—Insights from closed-system pyrolysis experiments. International Journal of Coal Geology, 154–155: 213–239

Wang Dongdong, Dong Guoqi, Zhang Gongcheng, et al. 2020. Coal seam development characteristics and distribution predictions in marginal sea basins: Oligocene Yacheng Formation coal measures, Qiongdongnan Basin, northern region of the South China Sea. Australian Journal of Earth Sciences, 67(3): 393–409, doi: 10.1080/08120099.2019.1661286

Wang Zhengfeng, Jiang Tao, Zhang Daojun, et al. 2015a. Evolution of deepwater sedimentary environments and its implication for hydrocarbon exploration in Qiongdongnan Basin, northwestern South China Sea. Acta Oceanologica Sinica, 34(4): 1–10, doi: 10.1007/s13131-015-0645-4

Wang Ce, Liang Xinquan, Foster D A, et al. 2016. Zircon U-Pb geochronology and heavy mineral composition constraints on the provenance of the middle Miocene deep-water reservoir sedimentary rocks in the Yinggehai-Song Hong Basin, South China Sea. Marine and Petroleum Geology, 77: 819–834, doi: 10.1016/j.marpetgeo.2016.05.009

Wang Zhengfeng, Liu Zhen, Cao Shang, et al. 2014a. Vertical migration through faults and hydrocarbon accumulation patterns in deepwater areas of the Qiongdongnan Basin. Acta Oceanologica Sinica, 33(12): 96–106, doi: 10.1007/s13131-014-0579-2

Wang Zhengfeng, Shi Xiaobin, Yang Jun, et al. 2014b. Analyses on the tectonic thermal evolution and influence factors in the deepwater Qiongdongnan Basin. Acta Oceanologica Sinica, 33(12): 107–117, doi: 10.1007/s13131-014-0580-9

Wang Zhengfeng, Sun Zhipeng, Zhang Daojun, et al. 2015b. Geology and hydrocarbon accumulations in the deepwater of the northwestern South China Sea—with focus on natural gas. Acta Oceanologica Sinica, 34(10): 57–70, doi: 10.1007/s13131-015-0715-7

Wang Zhenfeng, Sun Zhipeng, Zhu Jitian, et al. 2015c. Natural gas geological characteristics and great discovery of large gas fields in deep-water area of the western South China Sea. Natural Gas Industry B, 2(6): 489–498, doi: 10.1016/j.ngib.2016.03.001

Wang Dongdong, Zhang Gongcheng, Li Zengxue, et al. 2021. The development characteristics and distribution predictions of the Paleogene coal-measure source rock in the Qiongdongnan Basin, northern South China Sea. Acta Geologica Sinica (English Edition), 95(1): 105–120, doi: 10.1111/1755-6724.14625

Webster P J. 1994. The role of hydrological processes in ocean-atmosphere interactions. Reviews of Geophysics, 32(4): 427–476, doi: 10.1029/94RG01873

Wingert W S, Pomerantz M. 1986. Structure and significance of some twenty-one and twenty-two carbon petroleum steranes. Geochimica et Cosmochimica Acta, 50(12): 2763–2769, doi: 10.1016/0016-7037(86)90225-5

Wu Piao, Hou Dujie, Gan Jun, et al. 2018a. Paleoenvironment and controlling factors of Oligocene source rock in the eastern deep-water area of the Qiongdongnan Basin: evidences from organic geochemistry and palynology. Energy & Fuels, 32(7): 7423–7437

Wu Xiaochuan, Pu Renhai, Chen Ying, et al. 2018b. Seismic analysis of early-mid Miocene carbonate platform in the southern Qiongdongnan Basin, South China Sea. Acta Oceanologica Sinica, 37(2): 54–65, doi: 10.1007/s13131-017-1128-6

Wu Guoxuan, Qin Jungan, Mao Caizhi. 2003. Deep-water Oligocene pollen record from South China Sea. Chinese Science Bulletin, 48(22): 2511–2515

Xiao Xianming, Xiong M, Tian Hui, et al. 2006. Determination of the source area of the Ya13–1 gas pool in the Qiongdongnan Basin, South China Sea. Organic Geochemistry, 37(9): 990–1002, doi: 10.1016/j.orggeochem.2006.06.001

Xu Min, Hou Dujie, Lin Xiaoyun, et al. 2022. Organic geochemical signatures of source rocks and oil-source correlation in the Papuan Basin, Papua New Guinea. Journal of Petroleum Science and Engineering, 210: 109972, doi: 10.1016/j.petrol.2021.109972

Yang Gengxiong, Yin Hongwei, Gan Jun, et al. 2022. Explaining structural difference between the eastern and western zones of the Qiongdongnan Basin, northern South China Sea: insights from scaled physical models. Tectonics, 41(2): e2021TC006899

Zhang Gongcheng, Wang Dongdong, Zeng Qingbo, et al. 2019. Characteristics of coal-measure source rock and gas accumulation belts in marine-continental transitional facies fault basins: A case study of the Oligocene deposits in the Qiongdongnan Basin located in the northern region of the South China Sea. Energy Exploration & Exploitation, 37(6): 1752–1778

Zhang Gongcheng, Zeng Qingbo, Su Long, et al. 2016. Accumulation mechanism of LS 17–2 deep water giant gas field in Qiongdongnan Basin. Acta Petrolei Sinica, 37(S1): 34–46

Zhao Rui, Chen Si, Olariu C, et al. 2019. A model for oblique accretion on the South China Sea margin; Red River (Song Hong) sediment transport into Qiongdongnan Basin since upper Miocene. Marine Geology, 416: 106001, doi: 10.1016/j.margeo.2019.106001

Zhao Meng, Shao Lei, Liang Jianshe, et al. 2015. No Red River capture since the late Oligocene: Geochemical evidence from the northwestern South China Sea. Deep-Sea Research Part II: Topical Studies in Oceanography, 122: 185–194, doi: 10.1016/j.dsr2.2015.02.029

Zhou Yi, Sheng Guoying, Fu Jiamo, et al. 2003. Triterpane and sterane biomarkers in the YA13–1 condensates from Qiongdongnan Basin, South China Sea. Chemical Geology, 199(3–4): 343–359

Zhu Weilin, Shi Hesheng, Huang Baojia, et al. 2021. Geology and geochemistry of large gas fields in the deepwater areas, continental margin basins of northern South China Sea. Marine and Petroleum Geology, 126: 104901, doi: 10.1016/j.marpetgeo.2021.104901

Zhu Yangming, Sun Linting, Hao Fang, et al. 2018. Geochemical composition and origin of Tertiary oils in the Yinggehai and Qiongdongnan Basins, offshore South China Sea. Marine and Petroleum Geology, 96: 139–153, doi: 10.1016/j.marpetgeo.2018.05.029

Appendix: Structures of some compounds mentioned in the text

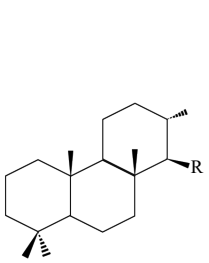

I tricyclic terpanes

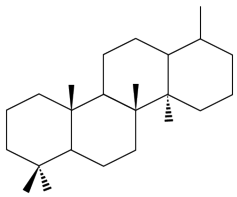

II C_{24} tricyclic terpanes

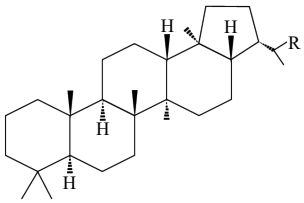

III hopanes

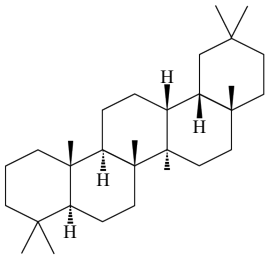

IV oleanane

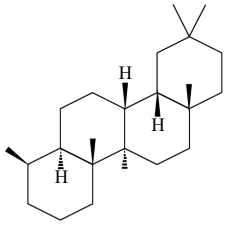

V *des*-A-oleanane

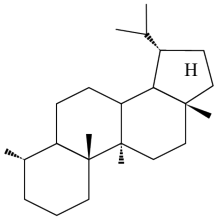

VI *des*-A-lupane

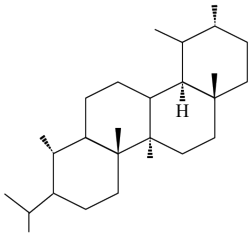

VII *des*-A-ursane

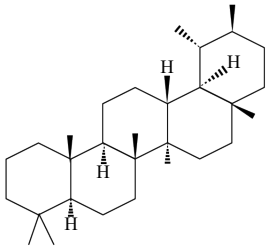

VIII taraxastane

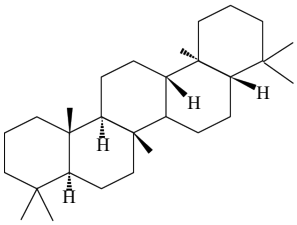

IX gammacerane

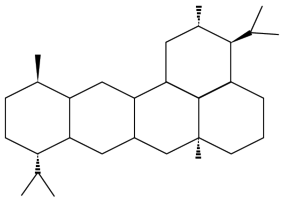

X cis-cis-trans-bicadinane (W)

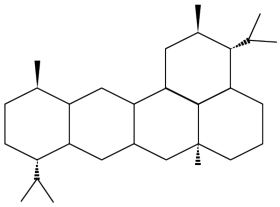

XI trans-trans, trans-bicadinane (T)

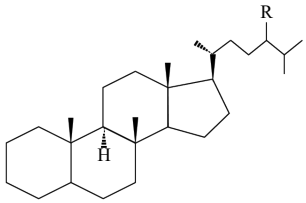

XII steranes